https://doi.org/10.5194/egusphere-2026-6201
Preprint. Discussion started: 3 November 2026
© Author(s) 2026. CC BY 4.0 License.

Characterizing spatially heterogeneous and homogeneous low-level mixed phase clouds over the Arctic using in situ measurements

John J. D'Alessandro[1,*], Odran Sourdeval[1], Olivier Jourdan[2], Antoine Baudoux[2], Aymeric Dziduch[2], Guillaume Mioche[2], Manuel Moser[3]

[1]Laboratoire d'Optique Atmosphérique (LOA), UMR 8518, CNRS, Université de Lille, 59000 Lille, France
[2]Laboratoire de Météorologie Physique (LaMP)/OPGC, Université Clermont Auvergne, CNRS/UMR 6016, Clermont-Ferrand, France
[3]Institut für Physik der Atmosphäre, Deutsches Zentrum für Luft- und Raumfahrt, Weßling, Germany

Correspondence to: John J. D'Alessandro (john.d-alessandro@univ-lille.fr)

Abstract.

Polar mixed phase clouds (MPCs) are notoriously difficult to represent in models of varying scales; and can be difficult to characterize with varying observational platforms. Accurate measurements/characterizations of MPCs are therefore vital to improve our understanding of them. This study uses airborne, in situ measurements acquired during three field campaigns to examine cloud phase properties and the spatial heterogeneity of Arctic MPCs. Cloud phase is diagnosed using a novel methodology incorporating a Bayesian Gaussian Mixture Model. To determine how the proposed methodology compares with previously developed classification methods, cloud phase occurrence frequencies are compared between four different methodologies. Large differences exist based on methodological approach, warranting future intercomparisons.

This study introduces three MPC types which classify consecutive 1 Hz in-cloud measurements as 1) liquid-dominated (containing only liquid and mixed phase samples), 2) ice-dominated (containing only ice and mixed phase samples) and 3) phase-segregated (containing liquid and ice phase samples), which are the least common. Liquid-dominated MPCs are more spatially heterogeneous than ice-dominated MPCs.

Discretizing MPC measurements into these categories may help disentangle complex relationships between physical factors controlling MPCs. For example, we evaluate differences of spatially heterogeneous and homogenous MPCs by controlling for the frequency occurrence of different cloud phases within MPCs. Spatially heterogeneous liquid-dominated MPCs have higher (lower) concentrations of large droplets (ice crystals) having diameters ~25–60 μm (>~1000 μm) than spatially homogeneous MPCs. Minor differences are observed for turbulent kinetic energy; whereas heterogeneous MPCs preferentially occur from -10° to -5°C.

https://doi.org/10.5194/egusphere-2026-6201
Preprint. Discussion started: 3 November 2026
© Author(s) 2026. CC BY 4.0 License.

1 Introduction

Low-level, mixed phase clouds (i.e., clouds containing both liquid and ice particles; MPCs) are commonly observed over the Arctic Ocean (Dziduch et al., 2026b; Matus and L'Ecuyer, 2017; Mioche et al., 2015). Their canonical structure consists of a single cloud layer having a thin layer of supercooled liquid overly a region of precipitating ice (Boer et al., 2009; Korolev et al., 2017; Morrison et al., 2012; Shupe et al., 2006), but they also occur as multiple, distinct cloud layers (Shupe, 2011; Shupe et al., 2006; Wallentin et al., 2026) as well as multiple layers of liquid and ice particles embedded within the same cloud (e.g., Luke et al., 2010). Polar MPCs have been notoriously difficult to simulate in models of varying resolutions (Schulte et al., 2026; Shaw et al., 2022), requiring accurate observations for model evaluation. Such observations are especially important given rapidly increasing temperatures in the Arctic region (i.e., Arctic Amplification) (Druckenmiller et al., 2025; Wendisch et al., 2024); and the sensitivity of regional temperatures to the presence and properties of MPCs (Bertrand et al., 2025).

Questions remain concerning how MPCs can persist for days and even weeks, regardless of being thermodynamically unstable due to the coexistence of liquid and ice particles (Morrison et al., 2012), given that ice particles grow at the expense of liquid droplets via the Wegener-Bergeron-Findeisen process (Bergeron, 1935; Findeisen, 1938; Wegener, 1911). However, the efficiency of this process is highly dependent on how liquid and ice crystals are spatially distributed within an MPC. Regions having liquid and ice particles well inter-mixed will be associated with greater rates of liquid depletion than regions where these particles are spatially isolated (e.g., Tan and Storelvmo, 2016; Zhang et al., 2019). Additionally, there are differences in the radiative properties of MPCs due to variability in the spatial distribution of ice and liquid particles (Ruiz-Donoso et al., 2020), as well as variability in the overall phase partitioning (e.g., Cesana and Storelvmo, 2017; Sun and Shine, 1994). Variability in phase partitioning additionally impacts cloud lifetimes and precipitation efficiency (e.g., Suzuki et al., 2024).

Numerous studies have recently quantified the cloud phase spatial heterogeneity of polar clouds (e.g., Coopman and Tan, 2023; D'Alessandro et al., 2021; Dammann et al., 2025; Deng et al., 2024; Sokol and Storelvmo, 2024; Yang et al., 2024), some of which relate the degree of heterogeneity to varying parameters such as temperature and turbulent motion. One study found that the distribution of phase lengths approximately follows a -5/3 power law (Korolev and Milbrandt, 2022), consistent with the scaling expected for quantities governed by the inertial-range energy cascade in turbulent motion (Kolmogorov, 1991). However, further characterization of MPC properties in the context of their spatial heterogeneity is crucial for model parameterization and improved understanding of MPC evolutionary pathways. For example, questions remain concerning the prevalence of primary and secondary ice nucleation (Kanji et al., 2017; Korolev and Leisner, 2020), both of which are intimately related to cloud phase spatial heterogeneity. Relevant questions include 1) What cloud phase occurrence frequencies are associated with more spatially heterogeneous MPCs compared with more homogeneous MPCs, and 2) What differences are observed in the microphysical properties and ambient conditions of more spatially

https://doi.org/10.5194/egusphere-2026-6201
Preprint. Discussion started: 3 November 2026
© Author(s) 2026. CC BY 4.0 License.

heterogeneous MPCs compared with more homogeneous MPCs? Addressing these questions should shed light on how ice formation/microphysical processes can influence phase spatial heterogeneity, and more broadly the lifecycles of MPCs.

This study addresses the two questions above, as well as evaluates other cloud phase and MPC characteristics using in situ measurements over the Arctic Ocean acquired during three field campaigns based out of Svalbard, Norway. To aid in the analysis, this study will introduce distinct MPC types defined by their spatial distributions of liquid and ice particles. This study also includes a cloud phase classification comparison between the one proposed here and previously published classification algorithms. The following section introduces the instrumentation and cloud phase classification methodology. Section 3 presents findings of cloud phase frequency occurrence, the introduction of the aforementioned MPC types and other MPC characteristics in the context of their spatial heterogeneity. Section 4 provides detailed discussion of the findings and Section 5 presents concluding remarks.

2 Instrumentation and methodology

2.1 Instrumentation and field measurements

In situ measurements used here were acquired during three field campaigns in the Arctic: 1) Airborne measurements of radiative and turbulent FLUXes of energy and momentum in the Arctic boundary layer (AFLUX), 2) the MOSAiC Airborne observations in the Central Arctic (MOSAiC-ACA) campaign, which was the airborne component of the Multidisciplinary drifting Observatory for the Study of Arctic Climate (MOSAiC) project and 3) the Arctic Amplification: Climate relevant atmosphere and surface processes and feedback mechanisms (HALO-AC3) campaign. All of the campaigns were based out of Svalbard, Norway, and targeted low-level clouds over open ocean and sea ice. AFLUX took place in March and April of 2019, MOSAiC-ACA took place in September, 2020 and HALO-AC3 took place in March and April of 2022. In situ measurements from HALO-AC3 are taken from the Polar-6 aircraft (three aircraft were deployed during this campaign). All Details of flight instrumentation and deployment strategy for AFLUX and MOSAiC-ACA are found in Mech et al. (2022); and similar details for the HALO-AC3 campaign are found in Ehrlich et al. (2025). in situ measurements are reported at 1 Hz resolutions, resulting in horizontal spatial resolutions ~60 m (depending on flight speed).

Cloud particle size distributions (PSDs) are obtained by merging measurements from either a Cloud Droplet Probe (CDP) or Cloud Aerosol Spectrometer (CAS) with a 2-Dimension imaging Stereo Probe (2DS), and Precipitation Imaging Probe (PIP). Measurements from a CDP were acquired during MOSAiC-ACA and HALO-AC3, whereas CAS measurements were acquired during AFLUX. The merged PSD product reports particles having diameters ranging from 2–6400 µm. Details on how the measurements were merged can be found in Dziduch et al. (2026a). Unless specified otherwise, all microphysical parameters are derived from the PSDs. This includes parameters such as the number- and volume-weighted mean diameter (*Mean D* and *MVD,* respectively) and the standard deviation of particle diameters (σ_D). Droplet size distributions and ice

https://doi.org/10.5194/egusphere-2026-6201
Preprint. Discussion started: 3 November 2026
© Author(s) 2026. CC BY 4.0 License.

particle size distributions were also derived from these measurements, where all particles having D<50 µm and spherical particles having diameters (D) from 50–300 µm are liquid (determined using the circularity parameter following Crosier et al. (2011)). Two parameters used in this study are derived from these phase-specific PSDs, namely, liquid water content divided by the total water content (*LWC/TWC*), and the extinction coefficient of liquid droplets in the visible wavelength domain over the extinction of all particles (β_l/β). The *LWC* is derived from the drop size distributions assuming spherical particles, whereas the ice water content is derived from the ice particle size distributions following the mass-dimension relationship proposed by Hogan et al. (2012). A Polar Nephelometer was available during all three campaigns, which measures the scattering phase function of a set of cloud particles from which the asymmetry parameter (g) is derived, in order to diagnose cloud phase (Gayet et al., 1997; Jourdan et al., 2010). In this study, in-cloud samples are those having the total water content (liquid and frozen condensate; *TWC*) exceed 0.01 g m^{-3}. This results in ~25 hours of in-cloud measurements from the three field campaigns at temperatures where liquid and ice can coexist (-40° to 0°C).

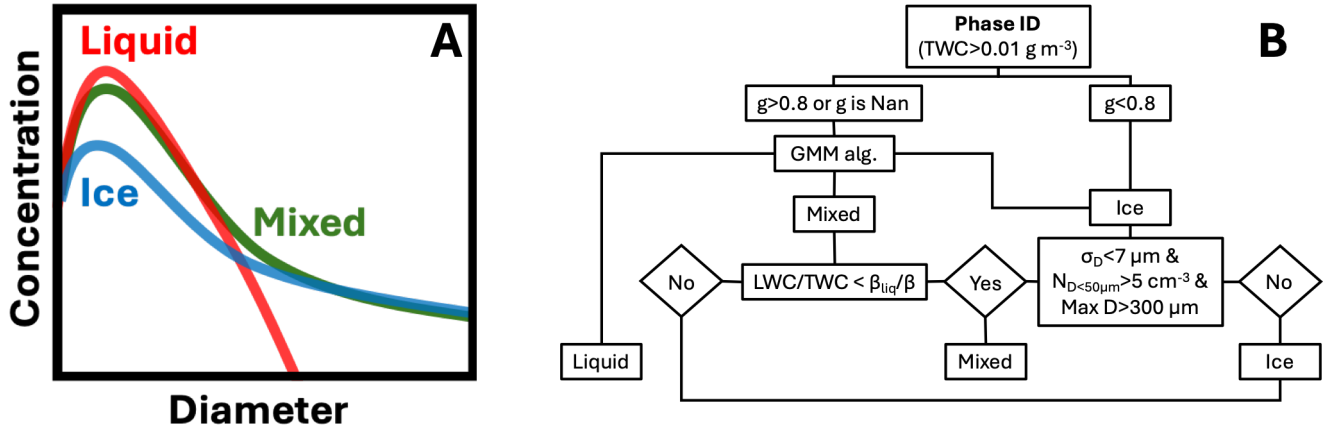
Meteorological measurements were obtained using a noseboom-mounted instrument package designed to measure airflow and thermodynamic variables having a high temporal resolution required for deriving turbulent fluxes. Three-dimensional wind components were measured with an Aventech Research Inc. five-hole probe coupled to an inertial navigation system, while air temperature measurements were provided by a fast-response open-wire Pt100 sensor. These measurements were complemented by slower-response Vaisala HMT-333 instruments, which provided air temperature, relative humidity and static pressure measurements. Meteorological variables, including pressure, three-dimensional wind vector components, air temperature, and humidity were recorded at 100 Hz, and are also available as 1 Hz temporally averaged products (Hartmann et al., 2018). To minimize measurement uncertainty associated with the wind component instrumentation, measurements are restricted to non-veering (|aircraft pitch|<1.5°), level flight legs (|Δ(height) / Δ(time)| < 2 m s^{-1}). During HALO-AC3, the Polar 5 aircraft flew over the in situ-sampling Polar 6 aircraft with a nadir-pointing High Spectral Resolution Lidar (Esselborn et al., 2008), acquiring cloud top measurements. However, the Polar 5 was unable to fly directly over the Polar 6 in order to avoid dropsonde deployments collisions. Because of this, cloud top retrievals are only used if obtained within 10 minutes and 2 km horizontally of the in situ measurements.

2.2 Cloud phase classification

Numerous studies have classified cloud phase using varying methods applied to varying in situ measurement platforms (Cober et al., 2001; Costa et al., 2017; D' Alessandro et al., 2019; Evans et al., 2025; Huang et al., 2021; Kirschler et al., 2023; Korolev et al., 2003; McFarquhar et al., 2007; Mioche et al., 2017; Moser et al., 2023), and many recent studies have used (primarily supervised) machine learning approaches for classifying particle phase and habit to ultimately classify a set of particles as a given phase (e.g., D'Alessandro et al., 2021; Dziduch et al., 2026b; Touloupas et al., 2020). Here we use a

https://doi.org/10.5194/egusphere-2026-6201
Preprint. Discussion started: 3 November 2026
© Author(s) 2026. CC BY 4.0 License.

125 "semi-supervised" machine learning approach to classify the cloud phase of each 1 Hz in-cloud sample. Unlike many previous machine learning methods, this approach is not applied to particle imagery/sphericity statistics to infer phase, but rather to varying parameters derived from cloud particle size distributions, liquid and ice particle size distributions, as well as scattering properties.



130 **Figure 1: A) Idealized depiction of expected PSD shapes for different cloud phase categories. B) The decision tree classifying cloud phase of 1 Hz measurements. The GMM alg. refers to the Gaussian Mixture Model discussed in the text.**

Figure 1A shows idealized depictions of the "archetypal" PSD shapes of liquid, ice and mixed phase samples in relation to each other (i.e., samples containing only liquid droplets, only ice particles, and a mixture of liquid and ice particles, 135 respectively). Liquid and mixed phase samples are generally expected to have higher concentrations of small particles, which here we define as those having D < 50 μm ($N_{D<50\mu m}$). Previous literature has used concentrations of these relatively small particles to diagnose the presence of liquid droplets (e.g., D'Alessandro et al., 2019, 2021; Finlon et al., 2019; Heymsfield et al., 2011; Lance et al., 2010), where concentrations exceeding ~1–10 cm^{-3} indicate the presence of liquid. In contrast, mixed and ice phase samples are generally expected to have larger concentrations of large particles (D > ~100–400 μm). This is 140 primarily because large drops having similar sizes are unexpected at supercooled temperatures due to concerns of aircraft icing (conditions which rarely occur in this region). Differences among different phases can be inferred from varying parameters derived from the PSDs, including *Mean D*, *MVD*, σ_D, *LWC/TWC* and β_l/β, which will be shown below. Figure 1B displays the cloud phase methodology, which includes a "semi-supervised" machine learning algorithm among other conditions (discussed in detail below). The methodology produces three cloud phase categories: liquid, ice and mixed. Due 145 to the chosen classes, the terminology in this study results in cloud phase being discussed in the context of three categories (liquid, ice and mixed phase), although there are only two phases of water condensate (liquid and ice phase).

https://doi.org/10.5194/egusphere-2026-6201
Preprint. Discussion started: 3 November 2026
© Author(s) 2026. CC BY 4.0 License.

Figure 2 examines these parameters in order to develop the proposed cloud phase classification methodology. Later on, distributions of select parameters will be shown to be associated with clear bimodalities corresponding to expected cloud phase classifications. Figure 2C shows a scatterplot of *g* and *LWC/TWC* colored by *MVD*. There are two clear modes of *g* at ~0.790 and ~0.845, and results here and in the overlying histogram displaying these results (2A) are overlaid with thresholds (dashed lines) denoting the phase classification following Mioche et al. (2017). Specifically, Mioche et al. (2017) classified all samples with $g<0.8$, $0.8<g<0.83$ and $g>0.83$ as ice, mixed and liquid phase samples, respectively. The bimodality clearly corresponds to scattering dominated by the ice and liquid phases, where the higher *g* mode has the highest *LWC/TWC*. However, relatively high *LWC/TWC* are also observed within the lower *g* mode (grey box). To validate whether these high *LWC/TWC* are associated with aspherical ice, we compare results with *RH* (with respect to water) to infer phase (2B), where *RH* peaking at liquid saturation would indicate the presence of liquid (e.g., Korolev and Isaac, 2006). However, the distribution does not peak at liquid saturation, suggesting the majority of these samples are ice phase and contain aspherical ice.

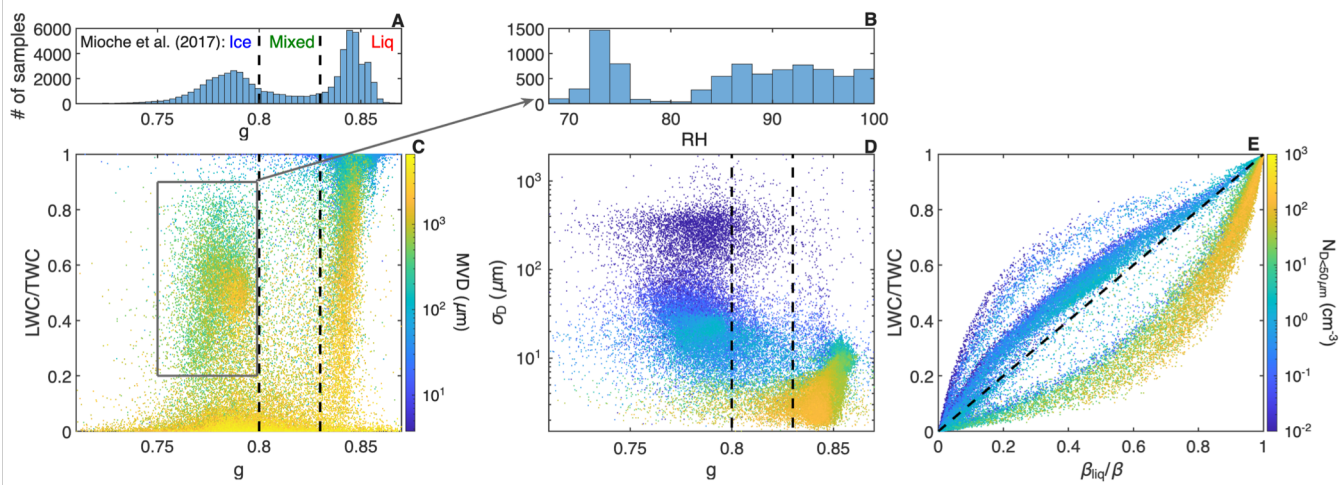


Figure 2: In-cloud measurements at 1Hz resolution displayed as A) Histogram of asymmetry parameter (g) from the Polar Nephelometer. B) Histogram of relative humidity with respect to liquid (RH) of a cluster of datapoints having relatively high LWC/TWC and g indicative of ice clouds. This cluster is located in C) which displays a scatterplot relating LWC/TWC and g; and datapoints are colored by mean volume-weighted diameter (MVD). Additional scatterplots show the PSD spread (σ_D) related to g in D) and LWC/TWC related the ratio of the liquid phase extinction over the summation of the liquid and ice phase extinction (β_l/β) in E). Datapoints in D) and E) are colored by the concentration of particles having D<50 μm ($N_{D<50\mu m}$). Vertical dashed lines in A,C,D correspond to threshold values of g used to classify cloud phase following Mioche et al. (2017). The dashed line in E is a 1:1 line.

https://doi.org/10.5194/egusphere-2026-6201
Preprint. Discussion started: 3 November 2026
© Author(s) 2026. CC BY 4.0 License.

Figure 2D shows a scatterplot of g and σ_D colored by $N_{D<50\mu m}$. High $N_{D<50\mu m}$ (indicative of droplets) are primarily observed at relatively high g (>0.83), and low $N_{D<50\mu m}$ (indicative of ice) are primarily observed at low g (<0.83). However, high $N_{D<50\mu m}$ also occur at g below 0.8 and low $N_{D<50\mu m}$ (indicative of ice) occur at g above 0.8, suggesting phase classification overlap within the mixed phase range of Mioche et al. (2017) ($0.8<g<0.83$), which will be revisited later on. Results show σ_D can be partly relied on as a proxy for cloud phase when g is not available (approximately one-third of measurements from the Polar Nephelometer are unavailable when $TWC>0.01$ g m^{-3}). Namely, greater σ_D corresponds to ice phase samples, which can be inferred by low $N_{D<50\mu m}$. This specifically corresponds to two modes, both of which have approximate centers at $g < 0.8$. Figure 2E shows a scatterplot of LWC/TWC and β_l/β colored by $N_{D<50\mu m}$, revealing two modes above and below the 1:1 line. These modes correspond with distinct differences in $N_{D<50\mu m}$ (orange datapoints below the 1:1 line and blue datapoints above the 1:1 line), highlighting how β_l/β can also be used to distinguish the different modes of high LWC/TWC observed in Figure 2C when Polar Nephelometer measurements are unavailable.

A "semi-supervised" Bayesian Gaussian Mixture Model (GMM) was developed based on these findings, which separates the in-cloud 1 Hz measurements into three classes: liquid, ice and mixed phase, based on their multivariate characteristics (represented by multivariate Gaussian distributions). GMMs are unsupervised clustering algorithms similar to k-means or hierarchical clustering, although they differ by allowing for "overlapping" datapoints in the same classes (i.e., soft clustering). Bayesian priors are selected for different model parameters to prevent overfitting and improve estimates while accounting for uncertainty, which will be shown later on. This approach incorporates posterior probabilities that given observations belong to each phase category, allowing for probabilistic rather than solely deterministic classifications (compared with a standard GMM). The input parameters include *Mean D*, *MVD*, $N_{D<50\mu m}$, σ_D, LWC/TWC, β_l/β and maximum particle diameter (*Max D*).

A subset of observations with "highly confident" phase assignments are also included in the GMM as anchors, i.e., those having a high degree of confidence in the diagnosed cloud phase; more so characterizing the model as "semi-supervised" rather than unsupervised. During each expectation step, the posterior membership probabilities of these anchor samples were highly constrained toward their prescribed classes before updating the model parameters. Consequently, the anchored samples influence the estimation of the class means and covariance matrices, which guide the classification of the remaining observations. This semi-supervised approach allows prior knowledge to be incorporated into the clustering process while retaining the flexibility to identify the underlying structure of the data. Anchors roughly correspond to expected PSD shapes and incorporate the asymmetry parameter (g) as follows:

1) Liquid phase: $g>0.83$ & $N_{D<50\mu m}>50$ cm^{-3} & *Max D*<150 µm
2) Mixed phase: $g>0.83$ & $N_{D<50\mu m}>10$ cm^{-3} & *Max D*>700 µm
3) Ice phase: $g<0.81$ & $\sigma_D>10$ µm

https://doi.org/10.5194/egusphere-2026-6201
Preprint. Discussion started: 3 November 2026
© Author(s) 2026. CC BY 4.0 License.

Based on the analysis for Figure 2, these anchor conditions all correspond to the respective phases with a high degree of confidence. The liquid phase is characterized by notably high small particle concentrations, a hard restriction on particle sizes and high asymmetry values indicative of liquid. Mixed phase samples are characterized by notably high small particle concentrations, sufficiently large particles which can confidently be diagnosed as ice crystals as well as high asymmetry values indicative of liquid. The high confidence in ice phase samples is derived from Figure 2D, where ice phase samples are generally broader due to the absence of high concentrations of small particles (confidently assumed to be droplets) as well as the low asymmetry values.

The GMM component of our classification approach is only applied to samples where g is either reported by the Polar nephelometer as exceeding 0.8 or is not reported. Samples having g<0.8 apply additional considerations to determine whether samples are ice phase or mixed phase. Note that two brute force conditions are applied following g<0.8 as well as the GMM component (Figure 1B). The first condition is to account for samples having g<0.8, where ice can be reclassified as mixed phase (or vice versa) based primarily upon σ_D and $N_{D<50\mu m}$. This is done to account for the fact that samples can contain liquid at g<0.8 (datapoints having $N_{D<50\mu m}$ > 10 cm^{-3} in Figure 2D). Relatively narrow σ_D are indicative of high small particle concentrations (i.e., droplets), and the *Max D* condition allows for relatively high concentrations of small ice to persist (occasionally observed at temperatures lower than -20°C). The second incorporates β_l/β to differentiate ice and mixed phase samples, since it was previously demonstrated that there are cases where high *LWC/TWC* can be ice phase (Figure 2C&E).

To evaluate the output of the model's classifications, Figure 3A,B,D,E shows histograms of varying parameters for the three cloud phase classes determined by the proposed methodology. Multimodal distributions are observed for all the parameters. The aforementioned priors used in the GMM roughly correspond to peak values observed in these panels. For example, the bimodal distribution of *Max D* is clearly separated into the liquid phase for smaller values (*Max D*<400 µm; dotted line) and the mixed and ice phases for larger values. Similarly, distributions of $N_{D<50\mu m}$ are clearly separated into the ice phase for lower values ($N_{D<50\mu m}$<5 cm^{-3}; dotted line) and the mixed and liquid phases for larger values. Perhaps interestingly, mixed phase samples have slightly greater $N_{D<50\mu m}$ than liquid phase samples, which may be unexpected due to the Wegener-Bergeron-Findeisen process. This will be revisited when examining PSDs of the different phase classifications in the following section.

https://doi.org/10.5194/egusphere-2026-6201
Preprint. Discussion started: 3 November 2026
© Author(s) 2026. CC BY 4.0 License.

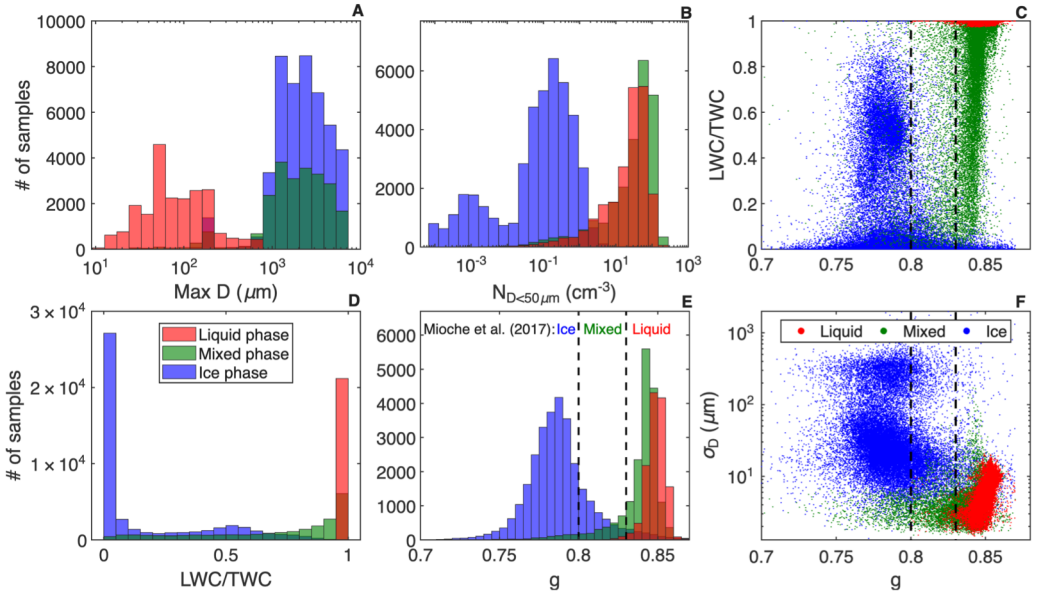


Figure 3: Histograms of 1Hz in-cloud measurements for separate cloud phases shown for A) the maximum particle diameter (Max D), B) the concentration of particles having D<50 µm ($N_{D<50µm}$), D) LWC/TWC and E) asymmetry parameter derived from the Polar Nephelometer (g). Scatterplots of LWC/TWC related to g and σ_D related to g are shown in C and F, respectively, both of which have datapoints colored by cloud phase. Vertical dashed lines in C,E,F correspond to threshold values of g used to classify cloud phase following Mioche et al. (2017). Note that C&F directly correspond to Figure 2C&D, respectively.

Additional histograms are shown for *LWC/TWC* (3D) and *g* (3E). The three phase classifications roughly correspond to the expected distributions, where liquid phase samples occur at $LWC/TWC \cong 1$, mixed phase samples at $0<LWC/TWC<1$ and ice phase samples at $LWC/TWC \cong 0$, although ice is also observed at relatively larger *LWC/TWC* which was discussed previously in relation to Figure 2C. This is displayed in Figure 3C, which is identical to 2C but colored by the phase classification. It is also important to note that the liquid phase is only observed at notably large *LWC/TWC* (exceeding 0.97) in Figure 3C, in contrast to previous studies relying on a threshold of $LWC/TWC>0.9$ for diagnosing liquid phase (e.g., D'Alessandro et al., 2019; Evans et al., 2025; Huang et al., 2021; Korolev and Milbrandt, 2022; Korolev et al., 2003; Korolev and Isaac, 2006), highlighting the greater sensitivity of the proposed methodology to the presence of ice for the mixed phase classification. This is similarly in contrast to Mioche et al. (2017), who classifies cloud phase based on the scattering signature of a sample of cloud particles, where liquid drops will dominate the scattering characteristics (which has been shown in different contexts; e.g., McFarquhar and Cober (2004)). Distributions of *g* in Figure 3E roughly correspond to Mioche et al. (2017), with liquid phase samples exceeding 0.83 and ice phase samples occurring the vast majority of the time below 0.8. However, there is overlap of the different phases extending beyond the threshold values of Mioche et al. (2017), most notably the high occurrence of mixed phase samples at $g>0.83$. Finally, Figure 3F shows a scatterplot of *g* and σ_D similar to Figure 2D but

https://doi.org/10.5194/egusphere-2026-6201
Preprint. Discussion started: 3 November 2026
© Author(s) 2026. CC BY 4.0 License.

colored by phase classification, showing it constrains the phase classification to the three modes: the two modes whose approximate centers are located at g<0.8 are classified as ice and the rightmost mode corresponds to liquid and mixed phase samples.

To conclude, the proposed cloud phase classification methodology primarily relies on parameters derived from the merged PSD products, since these parameters are input into the GMM. However, the Polar Nephelometer is also utilized for two purposes: 1) discretizing the cloud measurements into two groups which apply separate phase classification methods and 2) used as an anchor for stronger fitting to prescribed classes in the Gaussian Mixture Model method. This highlights the potential applicability of this methodology to other field campaigns using commonly deployed in situ instrumentation (e.g., spectrometers and optical imaging probes) together with some form of nominal phase discrimination measurements (e.g., hot-wire probes, vibrating icing rods).

3 Results

3.1 Phase frequencies and phase classification comparison

Figure 4 shows the relative cloud phase occurrence frequencies at different temperatures from the proposed phase classification methodology (4A), the previous phase classification proposed in Mioche et al. (2017) (4B), a previous phase classification proposed in Moser et al. (2023), which is modified in this study (4C), and a phase classification developed from measurements of Southern Ocean clouds in D'Alessandro et al. (2019), which has been used to classify cloud phase at varying regions globally (e.g., Wang et al., 2024; Yang et al., 2021; Zhang et al., 2019) (4D). All four methods capture expected trends that the frequency of liquid (ice) phase samples generally decrease (increase) with decreasing temperature. However, there are clear differences amongst the methodologies. As previously discussed, Mioche et al. (2017) diagnoses a larger fraction of samples as liquid phase compared to the proposed methodology which diagnoses a larger fraction as being mixed phase. It is important to note that the Polar Nephelometer does not detect particles having D > ~500–800 µm (Gayet et al., 1997; Mioche et al., 2017), suggesting it misses large ice crystals. Additionally, Mioche et al. (2017) has a lower relative frequency of ice samples. Supplementary Figure 1 shows this is at least partly attributed to a possible detection bias, where a greater frequency of ice phase samples are observed when data is missing from the Polar Nephelometer. Results in Figure 4E–H show PSDs averaged for the respective cloud phases. Using the Mioche et al. (2017) method (4F), we see a relatively similar number of particles having D>100 µm which never exceed a difference of a factor of 10 between liquid and mixed phase. This is in contrast to our methodology (4E) which has such particle concentrations notably diverge between the two phases. Further, notable differences exist in small drop concentrations between the two phases. For Mioche et al. (2017), particle concentrations are greater in liquid phase samples for all particles having D<100 µm. This is in contrast to our finding that the mixed phase has larger concentrations of particles having D<10 µm, discussed in the previous section (Figure 3B). Namely, results in Figure 4E show these higher drop concentrations in mixed phase samples (Figure 3B) are

https://doi.org/10.5194/egusphere-2026-6201
Preprint. Discussion started: 3 November 2026
© Author(s) 2026. CC BY 4.0 License.

attributed to greater drop concentrations having D<10 μm. We suspect this is due to a greater production of small droplets due to greater turbulent motion observed within mixed phase samples compared with liquid phase samples (not shown).

We move onto comparisons with a combined Moser et al. (2023) and Moser et al. (2026) approach. Moser et al. (2023) diagnosed cloud phase for samples acquired during AFLUX and MOSAiC-ACA by selecting modes within a joint histogram displaying occurrence frequencies of effective diameter and total cloud particle concentrations. This method relies on similar assumptions associated with cloud phase–PSD relationships previously discussed. Namely, liquid and mixed phase samples will generally have greater particle concentrations, and mixed and ice phase samples will generally have greater effective diameters. Moser et al. (2023) utilized a lower in-cloud mass content threshold to include subvisible clouds, and also limited their analysis to clouds below 500 m. Similarly plotting datapoints using our in-cloud conditions result in slightly varied modes compared with Moser et al. (2023). In order to adapt the methodology to this study, we slightly expand or modify the ranges of these modes, which are shown in Supplementary Figure 2. These modes were also slightly altered in a later study using HALO-AC3 measurements (Moser et al., 2026).

Note that the traditional liquid, ice and mixed phase categories are not used here. Rather, the ice phase includes samples from a previous mixed phase category in Moser et al. (2023) later classified as mixed phase haze in Moser et al. (2026) (dashed green and blue lines). This later study distinguishes "classical" MPCs with mixed phase haze, which they argue are coexisting ice particles and deliquesced aerosols. Phase frequencies from the modified Moser et al. (2023, 2026) approach reveal a notably high frequency of ice phase samples regardless of temperature. This method similarly captures lower concentrations of small drops for the mixed phase compared with liquid phase (D<7μm), similar to the proposed methodology. Supplementary Figure 3 shows results applying only the Moser et al. (2023) approach, and results when mixed phase haze is excluded.

We now focus on results from D'Alessandro et al. (2019), who classified cloud phase using a decision tree with threshold conditions separately applied to statistical parameters derived from particles less than and greater than 50 μm. In contrast to the other methods, D'Alessandro et al. (2019) approximately reproduces results from the proposed classification method. Namely, 83% of the sample classifications are in agreement from -20° to 0°C (in contrast to 37% for Mioche et al. (2017) and 30% for modified Moser et al. (2023, 2026)). Averaged PSDs also capture lower concentrations of particles having D < 10 μm for the liquid phase compared with mixed phase similar to the proposed methodology.

An additional point of discrepancy among the methodologies are the major differences in sample sizes, noting that Mioche et al. (2017) has proportionally two-thirds of the total sample size as the proposed methodology (due to its dependence on the Polar Nephelometer), and the modified Moser et al. (2023, 2026) has less than half the total number of samples compared with the proposed methodology (due to selecting samples from localized regions within the equivalent diameter–particle concentration phase space). These differences contribute to the relatively large percentage differences in phase frequencies

https://doi.org/10.5194/egusphere-2026-6201
Preprint. Discussion started: 3 November 2026
© Author(s) 2026. CC BY 4.0 License.

discussed in the previous paragraph. Overall, results highlight that caution should be taken when classifying cloud phase, in that phase classifications can vary widely amongst different methodologies which rely on similar assumptions.

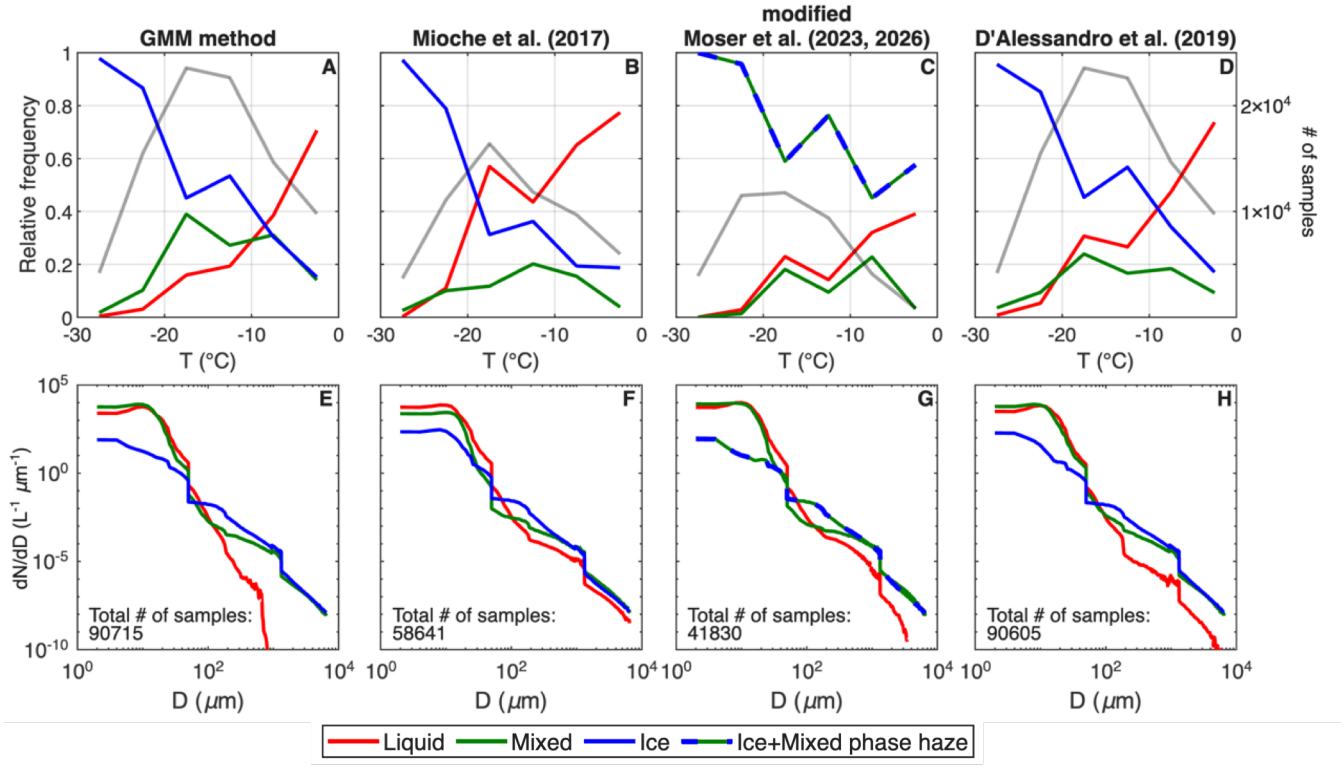


Figure 4: Relative cloud phase occurrence frequencies using the cloud phase classification methods from A) the Gaussian Mixture Model used in this study, B) Mioche et al. (2017), C) A modified version of Moser et al. (2023, 2026) and D) the simplified cloud phase classification (discussed in the text). Results are shown for different temperature ranges. Panels E–H show average particle size distributions (PSDs) for the different cloud phases corresponding to the respective, overlying cloud phase classification methodologies. The total number of available in-cloud samples from each methodology is included in these panels; whereas the number of samples for different temperature ranges is shown for the methodology used in this study by the gray line following the right ordinate in A.

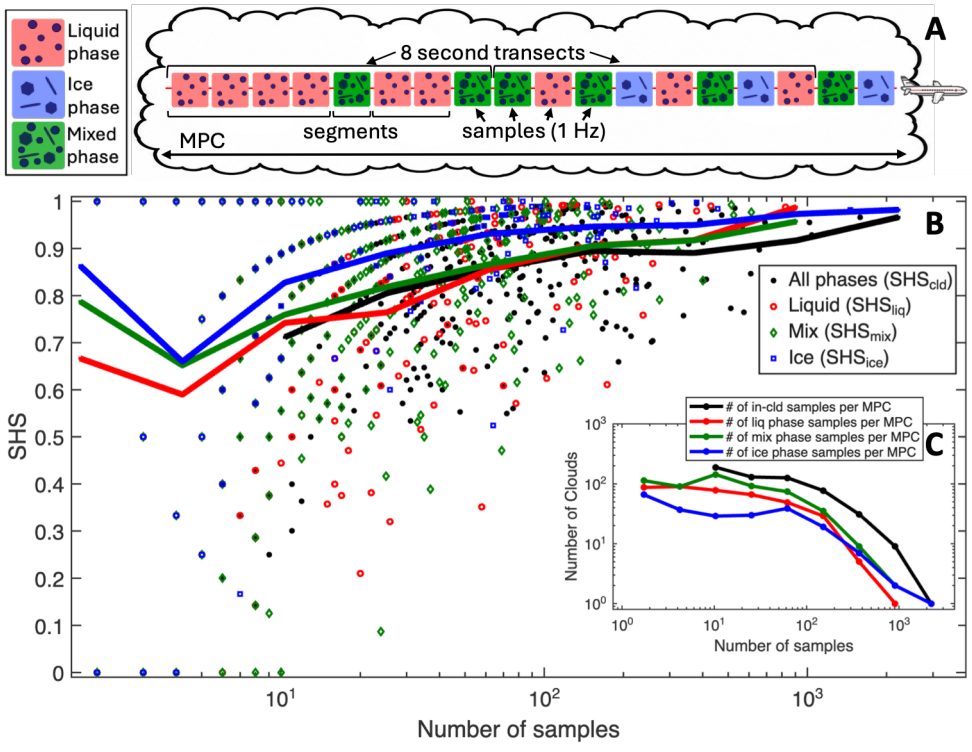
https://doi.org/10.5194/egusphere-2026-6201
Preprint. Discussion started: 3 November 2026
© Author(s) 2026. CC BY 4.0 License.

3.2 Cloud phase spatial heterogeneity

Previously, a spatial heterogeneity score (*SHS*) was introduced in D'Alessandro et al. (2021) which is a normalized measure of spatial heterogeneity. It is expressed as:

$$SHS = \frac{(Num_samples - Num_segments)}{(Num_samples - 1)}$$

Where Num_samples is the number of cloud samples in a cloud and Num_segments is the number of regions in a cloud where the neighboring samples have the same phase. An idealized depiction of samples and segments is shown in Figure 5A. Also included is the analytical definition for MPCs, which are 10 or more consecutive in-cloud samples ($TWC > 0.01$ g m^{-3}) where at least two different phases are observed. The equation can also be used to determine the spatial heterogeneity of individual phases as well, where Num_samples is the number of samples of a given phase and Num_segments is the number of regions in a cloud where neighboring samples have the given phase. Values of *SHS* approaching 1 (0) are more spatially homogeneous (heterogeneous). Figure 5B shows *SHS* computed over entire MPC lengths (SHS_{cld}; black markers) and for the respective phases within the clouds ($SHS_{liq,mix,ice}$; colored markers). Results are restricted to temperatures from -20°–0°C since ice phase samples dominate at colder temperatures (Figure 4A). All results for the remainder of this study are similarly restricted to -20°–0°C. Datapoints for SHS_{cld} are displayed as the number of consecutive in-cloud 1 Hz samples on the x-axis. Results for the different cloud phases simply shows the total number of samples of the respective phases in a given MPC.



https://doi.org/10.5194/egusphere-2026-6201
Preprint. Discussion started: 3 November 2026
© Author(s) 2026. CC BY 4.0 License.

Figure 5: A) Idealized depiction of the terms: Samples, Segments, MPCs and transects. The first three terms are used to compute cloud phase spatial heterogeneity, whereas transects are equidistant sets of consecutive, in-cloud samples. B) The cloud phase spatial heterogeneity of MPCs (SHS_{cld}) having varying cloud lengths denoted by the number of consecutive in-cloud samples (black markers). The colored markers show the spatial heterogeneity of the different cloud phases (SHS_{liq}, SHS_{mix}, SHS_{ice}) related to the number of samples of the given cloud phases within their respective clouds. C) The total number of samples. Results are restricted to temperatures from -20°–0°C.

The total number of MPCs and number of cloud phase samples within the MPCs are shown in Figure 5C. Averages for the respective *SHS* are shown as the solid lines in 5B. Note that the ice phase is the most spatially homogeneous, which is consistent with Korolev and Milbrandt (2022). In contrast, Korolev and Milbrandt (2022) found the mixed phase was more spatially inhomogeneous than the liquid phase, a finding not replicated here. However, if the proposed methodology is adjusted so that mixed phase samples with $LWC/TWC>0.9$ are reclassified as liquid phase (similar to Korolev and Milbrandt (2022)), the mixed phase clearly becomes the most spatially heterogeneous (Supplementary Figure S4). Further discussion of this is in Section 4.2. Sensitivity tests reveal consistent heterogeneity trends with those presented here when discretizing the dataset by 1) open ocean vs sea ice and 2) parallel vs perpendicular to the prevailing wind direction (not shown).

3.3 Introducing new MPC types

Before continuing the spatial heterogeneity analysis, novel classifications of MPCs (i.e., consecutive in-cloud samples containing at least two phases) are introduced to aid the remaining analyses of this study. Liquid-dominated MPCs are those where only liquid and mixed phase samples are observed as the aircraft passes through the cloud, and ice-dominated MPCs are those where only ice and mixed phase samples are observed. Phase-segregated MPCs are those where liquid and ice phase samples are observed in the same cloud. An idealized diagram of the three MPC types is shown in Figure 6A, which includes the relative frequencies of the MPC types and reveals that liquid-dominated MPCs occur most frequently (58%) and phase segregated MPCs occur least frequently (14%). This demonstrates that phase "overlap" of liquid and ice particles is extremely common, which has recently been suggested by Evans et al. (2025).

https://doi.org/10.5194/egusphere-2026-6201
Preprint. Discussion started: 3 November 2026
© Author(s) 2026. CC BY 4.0 License.

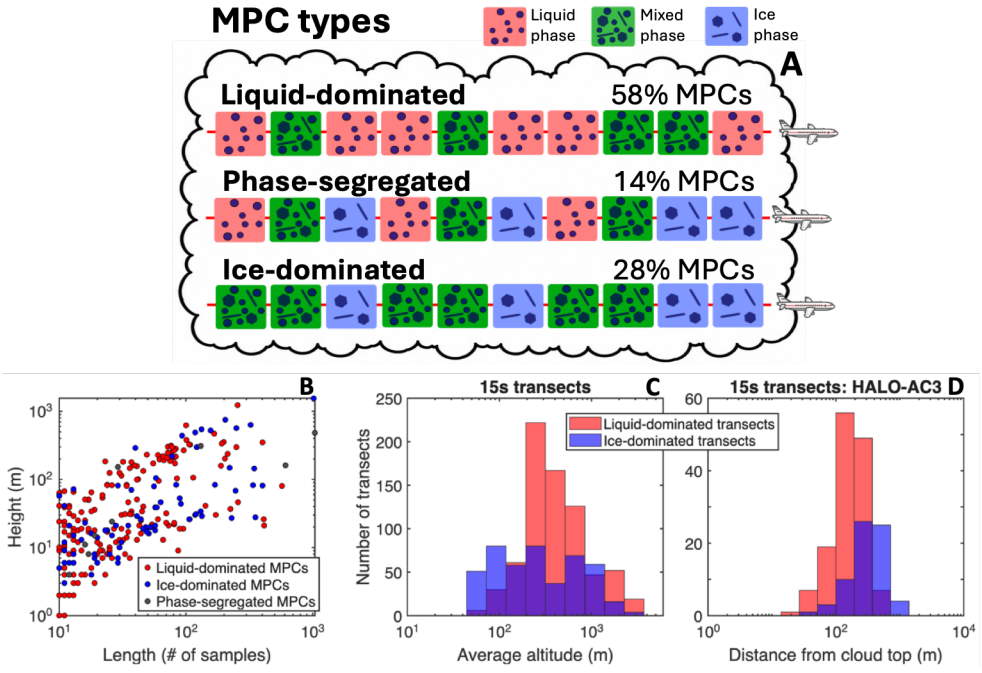


Figure 6: A) Idealized depictions of three MPC types. Percentages show the relative occurrence frequencies of these MPC types at temperatures from -20°–0°C. B) Length scales and vertical depths of MPC regime types. Liquid- and ice-dominated MPCs are restricted to 0.1<mixed phase normalized frequency<0.9 and phase-segregated MPCs are restricted to liquid phase normalized frequency>0.1 and ice phase normalized frequency >0.1. Panels C and D show histograms of transect height and distance from cloud top, respectively, for liquid- and ice-dominated transects. Transects are sets of 15 consecutive in-cloud measurements. Results in D are only shown from HALO-AC3, which had an overlying aircraft measure cloud top height with a nadir-pointing lidar (additional details in Section 2.1).

It is important to note that a one-dimensional sampling trajectory through a cloud is not necessarily representative of the phase characteristics of the total cloud volume. As previously mentioned, canonical single-layer MPCs in the Polar regions are vertically dispersed such that there is a thin layer of supercooled liquid overlying precipitating ice (e.g., Morrison et al., 2012; Shupe et al., 2006). Our terminology, which defines consecutive in-cloud samples as "MPCs," should rather be interpreted as localized regions within the cloud (although "MPC" is used here for simplicity). However, both liquid- and ice-dominated MPCs can extend well over 100 m vertically and over 10 km (assuming a flight speed of ~60 m s^{-1}) horizontally, as shown in Figure 6B where datapoints represent individual MPCs. Results in Figure 6B restrict cloud phase occurrence frequencies so that the MPC types are not overly dominated by a given cloud phase. Liquid- and ice-dominated MPCs are restricted to those having the relative frequency of mixed phase samples to all samples range from 0.1–0.9. Phase-segregated MPCs are restricted to liquid phase and ice phase normalized frequencies both exceeding 0.1. Much of the following analysis incorporates these cloud phase occurrence ratios when evaluating MPCs, which are discussed below.

https://doi.org/10.5194/egusphere-2026-6201
Preprint. Discussion started: 3 November 2026
© Author(s) 2026. CC BY 4.0 License.

Additional spatial statistics are provided in Figure 6C&D to contextualize MPC types relative to the clouds' 3-D structures, focusing on their vertical dimensions. Due to the variety of MPC vertical lengths, MPCs are split into regions of 15 consecutive in-cloud samples. These regions are defined as transects. Splitting measurements into transects has previously been performed in several contexts: to evaluate cloud phase spatial heterogeneity, the spatial heterogeneity of cirrus bulk microphysical properties and inferring the presence of significant entrainment-mixing (D'Alessandro et al., 2026, 2021, 2025). An idealized depiction of them is provided in Figure 5A. Note that they are not moving windows. Average cloud heights and distances from cloud top are shown for the liquid- and ice-dominated transects in Figure 6C&D, respectively. Note that transects in 6D are only included from HALO-AC3, as cloud top heights are derived from nadir-pointing lidar measurements mounted on an overlying aircraft during this campaign (details in Section 2.1). Ice-dominated transects have cloud height distributions shifted to slightly lower values than liquid-dominated transects. Additionally, ice-dominated transects have distributions of 'distance from cloud top' shifted to larger values respective to liquid-dominated transects. Considering the aforementioned canonical MPC structure, ice-dominated regions are likely associated with the precipitating-ice region, whereas liquid-dominated regions are likely associated with samples closer to cloud top. Future work further contextualizing these MPC types in varying MPC structures is warranted. Transects will be used later in Sections 3.4&3.5 when comparing heterogeneous and homogeneous MPCs.

Figure 7A shows histograms of the occurrence frequencies for different MPC types. Specifically, the histograms show relative occurrence frequencies of different phases within the MPCs on the x-axis; and these occurrence frequencies are relevant to different MPC types. For example, histograms of mixed phase normalized frequency are shown for liquid-dominated MPCs. This frequency parameter is the number of mixed phase samples divided by the total number of samples for each liquid-dominated MPC (red bars/x-axis label text). Note that in Figure 5A, the mixed phase normalized frequency would be 4/10 = 0.4. As the mixed phase normalized frequency increases, the number of liquid phase samples decreases as the number of mixed phase samples increases. Similarly, histograms of ice phase normalized frequency are shown for ice-dominated MPCs, which is the number of ice phase samples divided by the total number of samples (which in Figure 5A would be 4/10 = 0.4). As this normalized frequency increases, the number of mixed phase samples decreases as the number of ice phase samples increase (blue bars/x-axis label text). For phase-segregated MPCs, histograms are shown for the ratio of mixed and ice phase samples in the clouds, meaning the frequency of liquid phase samples decreases as the frequency of mixed and ice phase samples increases (i.e., mixed+ice phase normalized frequency; grey bars/black x-axis label text). All three metrics are characterized by a general decreasing (increasing) frequency of liquid (ice), or in other words: towards increasing glaciation. Distributions of the liquid- and ice-dominated MPC parameters display U-shaped distributions, although a relatively greater frequency of MPCs have ice phase normalized frequencies approaching 1 for ice-dominant MPCs, and similarly for phase-segregated MPCs. The absence of the normalized frequency parameters at ~0.5 suggests "gradual" transitions from initial nucleation to total glaciation of MPCs are relatively uncommon.

https://doi.org/10.5194/egusphere-2026-6201
Preprint. Discussion started: 3 November 2026
© Author(s) 2026. CC BY 4.0 License.

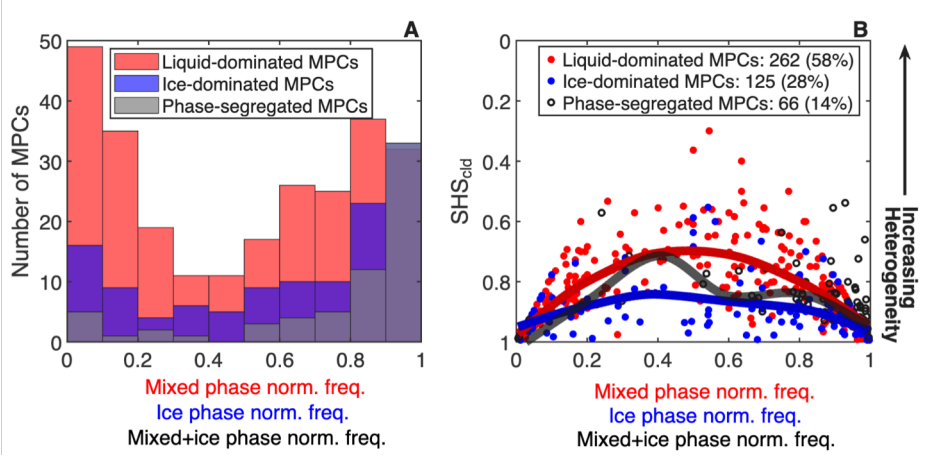


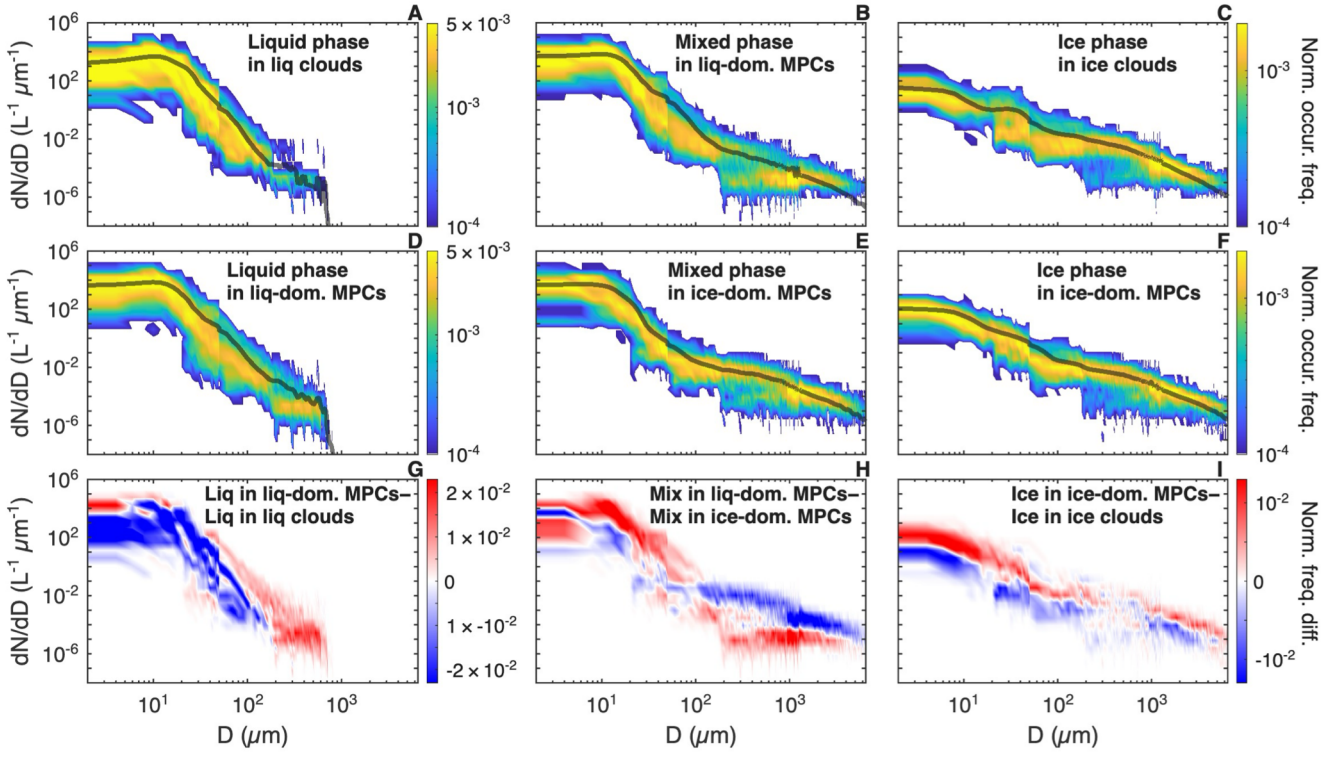
Figure 7: A) Histograms of cloud phase normalized frequencies for their relevant MPC types (discussed in the text). B) Scatterplot of SHS_{cld} for different MPC types. Solid lines are medians binned at cloud phase normalized frequencies of 0.2. Both panels plot results in relation to the relative cloud phase normalized frequencies relevant to their respective MPC types. For liquid-dominated MPCs, this is the ratio of mixed phase samples to all samples (mixed phase normalized frequency). For ice-dominated MPCs, this is the ratio of ice phase samples to all samples (ice phase normalized frequency). For phase-segregated MPCs, this is the ratio of mixed and ice phase samples to all samples (mixed+ice phase normalized frequency). Results are restricted to temperatures from -20°–0°C.

Figure 7B shows a scatterplot of the respective MPC types' normalized frequency parameters (similar to 7A) and their spatial heterogeneity. Specifically, SHS_{cld} is related all of the cloud phase normalized frequency parameters. The thick red, blue and grey lines show median SHS_{cld} values for the different cloud phase normalized frequencies of liquid-dominated, ice-dominated and phase-segregated MPCs, respectively. Note that SHS_{cld} decreases while ascending the y-axis, so datapoints higher in the panel are more spatially heterogeneous. The median lines show liquid-dominated MPCs are more spatially heterogeneous than ice-dominated MPCs, consistent with the general trends of cloud phase intermittency in Korolev and Milbrandt (2022) who show the liquid phase is more intermittent than the ice phase. This may be related to the greater resilience of ice particles to sublimation relative to droplets evaporating, especially if one assumes liquid saturation throughout the liquid-dominated MPCs and only localized regions of liquid saturation within ice-dominated MPCs (Korolev and Isaac, 2006). It may also indicate ice-dominated MPCs are generally more aged compared to liquid-dominated MPCs; and following this, have generally undergone more mixing which homogenizes the liquid and ice particles spatially.

Due to the relatively rare occurrence of phase-segregated MPCs/transects, we focus our attention on liquid- and ice-dominated MPCs/transects for the remainder of this study. Figure 8 shows joint histograms of PSDs of different phases from different cloud regime types, where the histograms are normalized over both dimensions such that the sum of all histogram bins across particle diameter and bin concentrations equals one. The left column shows PSDs of liquid phase samples in

https://doi.org/10.5194/egusphere-2026-6201
Preprint. Discussion started: 3 November 2026
© Author(s) 2026. CC BY 4.0 License.

liquid-only clouds (8A), liquid phase samples in liquid-dominated MPCs (8D) and a 2D display of the difference of these two plots (8G). The differences in the two liquid-phase categories reveal that liquid phase samples in liquid-dominated MPCs are generally broader, with greater concentrations of drops having D>~30 μm. This is consistent with much literature discussing similarly broader drop size distributions within mixed phase conditions (e.g., Cober et al., 2001; Korolev et al., 2003; Verlinde et al., 2013). The liquid-dominant MPC samples also have greater concentrations of smaller drops (D<~10 μm). This is consistent with the finding that mixed phase clouds tend to have higher concentrations of small drops compared to the liquid phase (Figure 4E), assuming the liquid phase samples possess similar drop size distributions of those in the neighboring mixed phase portions. The middle column shows PSDs of mixed phase samples from liquid-dominant MPCs (8B) and those from ice-dominant MPCs (8E). Differences in the two figures (8H) reveal mixed phase samples in liquid-dominant MPCs have higher concentrations of liquid drops (D<100 μm) and lower concentrations of relatively large ice (D>100 μm). The right column shows PSDs of ice phase samples from ice-only clouds (8C) and those within ice-dominated MPCs (8F). Their differences (8I) reveal that ice phase samples within ice-dominated MPCs generally contain larger concentrations of ice regardless of their size, suggesting the localized liquid-embedded samples provide a moisture source for maintenance/replenishment. Overall, results show distinct differences in the microphysical properties of these different MPC types.



https://doi.org/10.5194/egusphere-2026-6201
Preprint. Discussion started: 3 November 2026
© Author(s) 2026. CC BY 4.0 License.

Figure 8: Normalized joint frequency distributions of PSDs from A) liquid phase samples in clouds only containing liquid samples, B) mixed phase samples in liquid-dominated MPCs, C) ice phase samples in clouds only containing ice samples, D) liquid phase samples in liquid dominated MPCs, E) mixed phase samples in ice-dominated MPCs and F) ice phase samples in ice-dominated MPCs. The differences of the liquid phase samples, mixed phase samples, and ice phase samples from their respective cloud types are shown in G, H and I, respectively. Distributions are normalized by both particle size and concentrations. Grey lines denote the averaged PSDs. Results are restricted to temperatures from -20°–0°C.

3.4 Differences in microphysical properties of spatially heterogeneous and homogeneous MPCs

There is a notable amount of previous literature which characterizes the phase spatial heterogeneity of low-level clouds in the polar regions (references therein Section 1). However, there has been little work comparing the microphysical properties of spatially heterogeneous and homogeneous MPCs. Differences may elucidate key processes impacting glaciation, cloud lifetimes, as well as their general radiative properties. However, past studies comparing the properties of spatially heterogeneous and homogeneous clouds do not control for the frequency occurrence of different cloud phases, which may significantly bias results depending on the objective(s) of the analysis (e.g., Coopman and Tan, 2023; D'Alessandro et al., 2021; Deng et al., 2024; Sokol and Storelvmo, 2024). First, consider turbulent motion, which is an important factor for maintaining the presence of supercooled liquid in the presence of ice (e.g., Korolev and Field, 2008; Rauber and Tokay, 1991; Shupe et al., 2008). Not controlling for the frequency of mixed phase samples within a given MPC would therefore introduce an inherent bias when relating turbulent motion with spatial heterogeneity. For example, consider two liquid-dominated MPCs, where one is spatially homogeneous and one is spatially heterogeneous. If the homogeneous MPC composed primarily of liquid phase samples is compared with a heterogeneous MPC composed primarily of mixed phase samples, then the heterogeneous MPC would be biased towards greater turbulent motion. Similarly, the intimate relationship between cloud phase and temperature likely biases previous analyses correlating cloud phase heterogeneity with temperature, since relatively higher (lower) temperatures are inherently associated with significantly lower (greater) frequencies of ice. Such differences in phase frequencies could also bias similar analyses of the local microphysical properties. Considering the previous two MPCs example, the heterogeneous MPC would be biased towards larger particle sizes due to the presence of ice.

A methodology is proposed which controls for differences in cloud phase occurrence frequencies amongst different clouds. This method incorporates the usage of transects, and consists of three steps:

1. Find all transects having identical cloud phase occurrence frequencies.

https://doi.org/10.5194/egusphere-2026-6201
Preprint. Discussion started: 3 November 2026
© Author(s) 2026. CC BY 4.0 License.

2. Separate these transects into those with high spatial heterogeneity (*SHS*<50th percentile) and those with low spatial heterogeneity (*SHS*>50th percentile). Separately average the results of these two groups.
3. Repeat steps 1. and 2. for all possible combinations of cloud phase occurrence frequencies, then average results.

For MPCs containing all three cloud phase types, this would result in a very low number of available transects, since all three cloud phase frequencies have to be identical. However, we can take advantage of the high prevalence of liquid- and ice-dominated transects by considering only two cloud phase types. Additionally, splitting MPCs into equidistant regions significantly reduces the number of phase-segregated cases compared with the MPC statistics shown in Figure 5. For transects sizes in the following analysis (15, 25, and 35 seconds), this results in ~2–4% of all transects being characterized as phase-segregated (not shown). These transects are excluded from the analysis. For example, let's consider liquid-dominated transects having 15 consecutive samples (i.e., 15 seconds of in-cloud measurements). We first find all transects with 2 mixed phase samples and 13 liquid phase samples, which has a mixed phase normalized frequency of 2/15≅0.13 (step 1). We then separate these transects into "heterogeneous" and "homogeneous" transects using the median *SHS* as the threshold, where transects having *SHS* above (below) the median are classified as homogeneous (heterogeneous). Results are averaged for this mixed phase normalized frequency (separately for the heterogeneous and homogeneous transects) (step 2). Steps 1 and 2 are then repeated for 3 mixed phase samples and 12 liquid phase sample, and continually repeated for all possible mixed phase normalized frequency combinations (step 3). After repeating Steps 1 and 2 for all mixed phase frequency combinations, we then average the results over all possible combinations. This methodology ensures that results are not weighted by 1) varying frequencies of different cloud phase samples within a collection of transects as well as 2) the number of transects for a given cloud phase occurrence ratio (i.e., if the population of liquid-dominated transects contain mostly mixed phase samples rather than liquid phase samples, and vice versa). Note that phase frequency combinations are restricted such that neither cloud phase occurs over 90% of the time (e.g., for liquid-dominated MPCs, the mixed phase normalized frequency must be within 10%–90%).

The methodology is first used to evaluate differences of PSDs within heterogeneous and homogeneous liquid-dominated transects. A detailed depiction of how the methodology is implemented for evaluating PSDs is provided in the Appendix. It includes discussion of how PSDs are separately evaluated for mixed and the liquid phase samples, as well as discussion on how significance is computed. Figure 9 depicts differences in the PSDs by directly plotting the ratio of the PSDs' binned particle concentrations from heterogeneous transects over those from homogeneous transects. Values over 1 indicate the particle concentrations are greater in heterogeneous clouds compared with homogeneous clouds, and vice versa. The top row focuses on mixed phase PSDs and the bottom row focuses on liquid phase PSDs. To increase confidence in the analysis, two forms of sensitivity tests are performed here: 1) varying the transect lengths to be 15 seconds, 25 seconds and 35 seconds (red, green and blue lines, respectively) and 2) separately evaluating differences for liquid-dominated transects consisting mostly of liquid phase samples (mixed phase normalized frequency<0.5; middle column) and consisting mostly of mixed

https://doi.org/10.5194/egusphere-2026-6201
Preprint. Discussion started: 3 November 2026
© Author(s) 2026. CC BY 4.0 License.

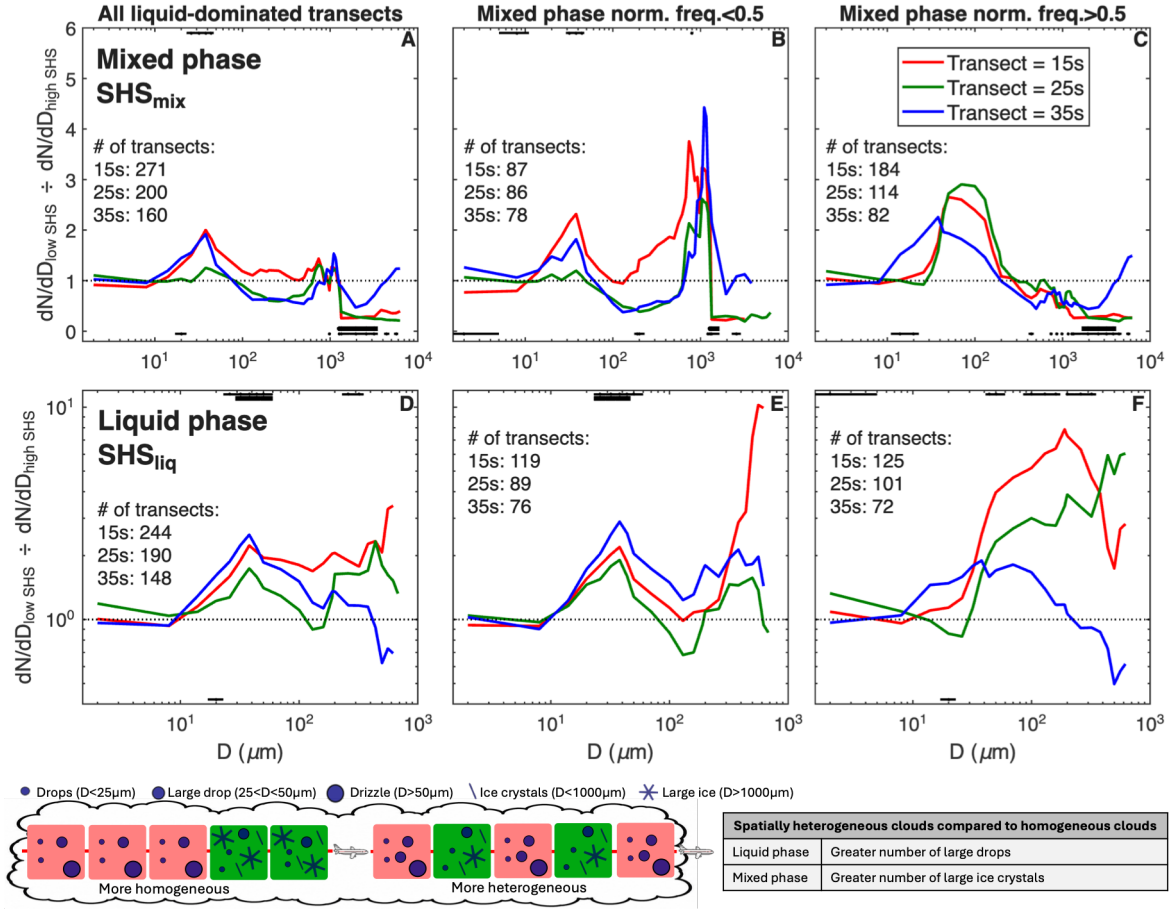
phase samples (mixed phase normalized frequency>0.5; right column). Results are relatively consistent between the different transect lengths for both cloud phases. Namely,

1) Liquid phase samples in heterogeneous transects have a greater number of drops with D~25–60 μm compared to homogeneous transects by a factor of ~2–3.
2) Mixed phase samples in heterogeneous transects have a lower number of ice crystals with D>~1000 μm compared to homogeneous transects by a factor of ~2–3.

Note that the overlying thick (thin) black lines denote bin widths where the ratios are significantly different for all three (only two) transect lengths, respectively, determined following the permutation method discussed in the Appendix. For overlying bars, this indicates particle concentrations in the heterogeneous transects are significantly greater than those in the homogeneous transects, and vice versa for the underlying bars. The two major trends listed above are significant for all transect lengths (thick black lines). An idealized depiction of these differences is provided underlying the panels in Figure 9.

The two major trends listed above are primarily associated with transects having different mixed phase normalized frequencies (9B,C,E,F). For example, greater frequencies of large drops having ~25<D<50 μm within the heterogeneous transects are only observed for transects composed primarily of liquid phase samples (mixed phase normalized frequency<0.5; middle column). Likewise, greater large ice concentrations are primarily found in homogeneous transects primarily composed of mixed phase samples (9C). Additionally, there are some minor differences in the trends among different transect lengths. For example, only two of the three transect lengths show significantly greater concentrations of drizzle droplets having 100<D<400 μm in the liquid phase samples (thin black line overlying ratios in 9F). Similarly, only two of the three transect lengths have greater large drop concentrations for the heterogeneous transects in mixed phase samples. Note that these trends are not included in the underlying idealized depiction of transect differences.

https://doi.org/10.5194/egusphere-2026-6201
Preprint. Discussion started: 3 November 2026
© Author(s) 2026. CC BY 4.0 License.



Spatially heterogeneous clouds compared to homogeneous clouds	
Liquid phase	Greater number of large drops
Mixed phase	Greater number of large ice crystals

Figure 9: The ratio of averaged PSD bin concentrations of liquid-dominated heterogeneous transects over those of homogeneous transects. Results are provided for mixed phase samples (A) and liquid phase samples (D). Results for the separate phases are also separately provided for transects containing mostly liquid phase samples (mixed phase norm. freq. < 0.5; B&E) and transects containing mostly mixed phase samples (mixed phase norm. freq. > 0.5; C&F), corresponding to their respective rows. Different colored lines correspond to the heterogeneity analysis being performed upon transects of different lengths. Thin lines denote bins with statistically significant ratios for two of the three transect sizes, and thick lines similarly denote statistical significance for all three transect sizes. The total number of transects used for each transect length are provided in the respective panels. The dashed lines are shown at the bin concentration ratios equal to one. An idealized depiction of signals displayed in A&D is shown underlying the panels, where red boxes are liquid phase samples and green boxes are mixed phase samples. The signals displayed are only of the proportionality of different particle concentrations for the MPC types. Results are restricted to temperatures from -20°–0°C.

https://doi.org/10.5194/egusphere-2026-6201
Preprint. Discussion started: 3 November 2026
© Author(s) 2026. CC BY 4.0 License.

Mixed phase and ice phase samples within ice-dominated MPCs are similarly evaluated in Figure 10. Large ice crystals concentrations (D>~100 µm) are approximately similar between heterogeneous and homogeneous transects, for both mixed and ice phase samples. Ice phase samples in heterogeneous transects have greater small ice concentrations (D<~100 µm) than in homogeneous transects by a factor of ~2–10. Mixed phase samples in heterogeneous transects have greater particle concentrations having ~30<D<100 µm than in homogeneous transects. Although we have low confidence in denoting the phase of these particles similar to the mixed phase samples in liquid-dominated transects, this is a similar signal observed for the liquid-dominated transects. Because of this, we assume droplets may be the primary phase of particles in this size range. Major trends are still observed regardless of the ice phase normalized frequency (not shown). An idealized depiction of these trends is shown underlying the panels.

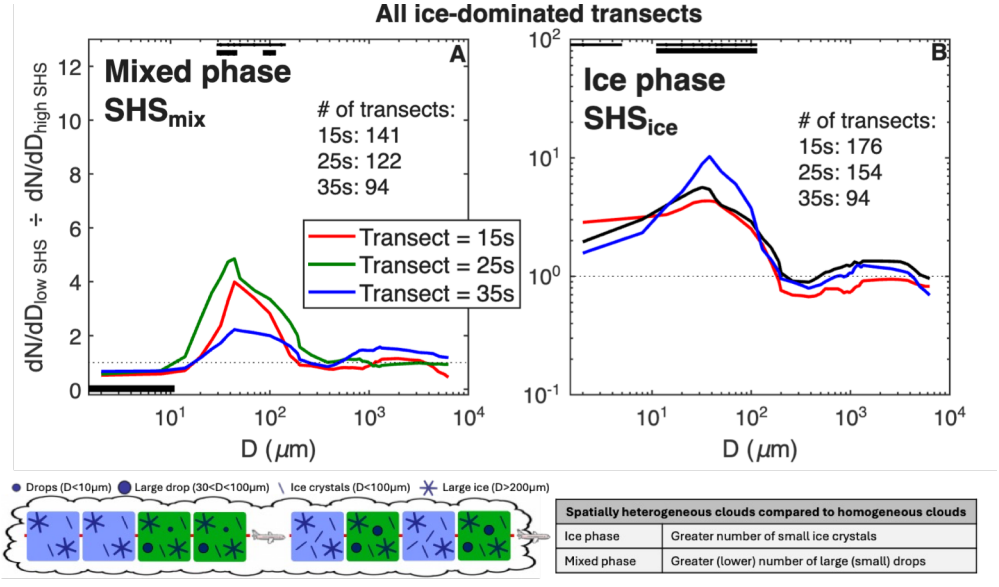


Figure 10: Similar to Figure 9A&D, except results are shown for ice-dominated transects. Mixed phase PSD bin concentration ratios are shown in A), and ratios for ice phase samples are in B). An idealized depiction of signals displayed in A&B is shown underlying the panels, where blue boxes are ice phase samples and green boxes are mixed phase samples. Results are restricted to temperatures from -20°–0°C.

Results in this section evaluated differences in the microphysical properties of spatially heterogeneous and homogenous transects within liquid-dominated and ice-dominated MPCs. For liquid-dominated MPCs, spatially heterogeneous transects have greater large drop concentrations (~25<D<60 µm) and lower large ice concentrations (D>~1000 µm) that homogenous transects. For ice-dominated MPCs, spatially heterogeneous transects have greater small ice concentrations (D<100 µm). Implications and further discussion of these findings are presented in Section 4.1.

https://doi.org/10.5194/egusphere-2026-6201
Preprint. Discussion started: 3 November 2026
© Author(s) 2026. CC BY 4.0 License.

3.5 Differences in ambient conditions of spatially heterogeneous and homogeneous MPCs

In this section, the methodology discussed in the previous section is applied to wind components and temperature measurements to observe possible correlations between cloud phase spatial heterogeneity (SHS_{cld}) and select ambient conditions. Turbulent motion is characterized using turbulent kinetic energy (*TKE*) and determined using the three-dimension wind components:

$$1)\ TKE = \frac{1}{2}(\sigma_u^2 + \sigma_v^2 + \sigma_w^2)$$

Where σ_u^2, σ_v^2 and σ_w^2 are the variance of the *u*, *v* and *w* wind components averaged for 1 Hz lengths, and determined over the transect lengths. The methodology is similar to that applied to the previous PSD analysis; but for each cloud phase normalized frequency, normalized frequency distributions are produced for 1 Hz *TKE* and temperature measurements (separate distributions for heterogeneous and homogeneous transects). The distributions from all possible cloud phase normalized frequencies are finally averaged to produce an average normalized occurrence frequency distribution. Note that this altered method similarly ensures results are not weighted by 1) varying frequencies of different cloud phase samples within a collection of transects as well as 2) the number of transects for a given cloud phase occurrence ratio. We show results over all liquid-dominated transects in Figure 11 for *TKE* (11A) and temperature (11B). The varying red (blue) distributions are for homogeneous (heterogeneous) transects having different transect lengths.

Only minor differences are observed in the distributions of *TKE* for heterogeneous and homogeneous transects regardless of transect length (11A). In contrast, it appears that notable differences exist between the occurrence of heterogeneity and inhomogeneous transects at different temperatures (11B). Namely, there is a greater frequency of heterogeneous transects at temperatures from -10° to -5°C compared with the homogeneous transects; and a greater frequency of homogeneous transects at temperatures from -20° to -15°C compared with heterogeneous transects. These differences are enhanced for transects primarily composed of liquid phase samples, where the frequency of heterogeneous transects at temperatures from -15° to -5°C is notably greater than the homogeneous transects (11C). No discernable differences in the heterogeneous and homogeneous transects are observed for transects composed primarily of mixed phase samples (11D). The following section provides detailed discussion on results presented here.

https://doi.org/10.5194/egusphere-2026-6201
Preprint. Discussion started: 3 November 2026
© Author(s) 2026. CC BY 4.0 License.

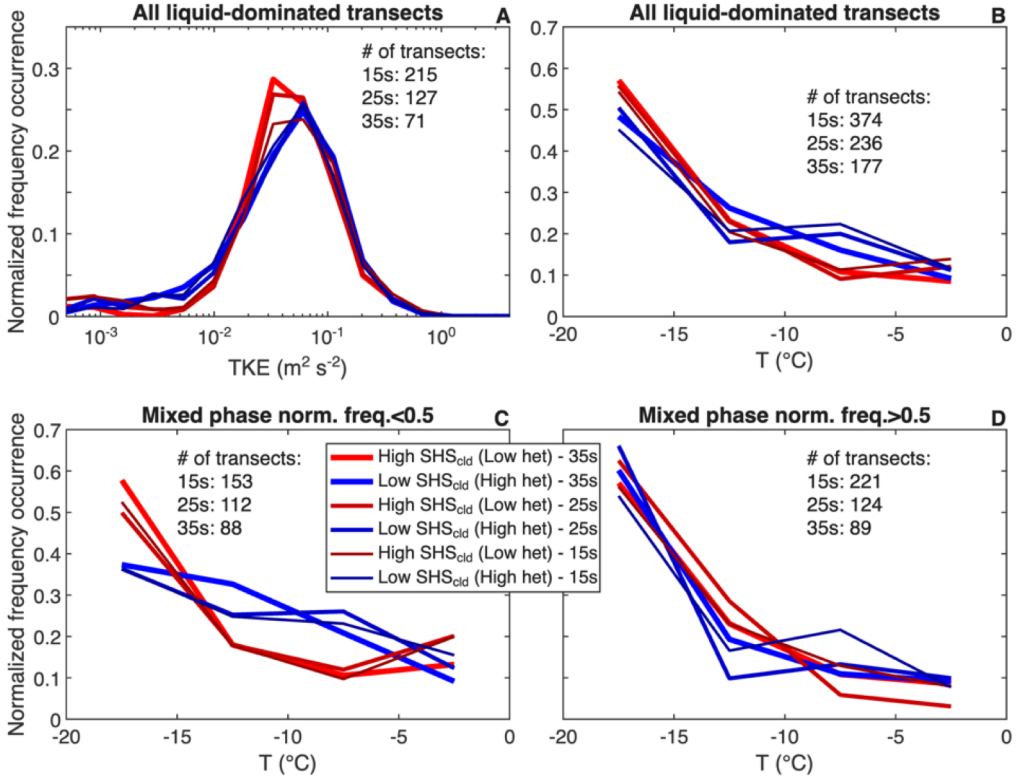


Figure 11: Normalized frequency distributions of A) TKE and B) temperature, where the blue and red distributions denote heterogenous and homogeneous transects, respectively. Varying color shades and linewidths denote different transect lengths. Distributions for temperature are also shown for liquid-dominated transects composed primarily of C) liquid phase samples and D) mixed phase samples. Results are restricted to temperatures from -20°–0°C.

Additional uncertainty in the wind measurements can result from computing the wind component perturbations on relatively short time scales. Highlighting this, the uncertainty analysis for AFLUX and MOSAiC-ACA wind components were performed over length scales on the order of kilometers (Ehrlich et al., 2019; Hartmann et al., 2018). To increase confidence in the analysis, an additional sensitivity test is provided in Supplementary Figure S5 which analyzes *TKE* computed over the length of the transects rather than at 1 Hz resolution (~100 m). Namely, the *u*, *v* and *w* wind components are averaged over 1 Hz, and *TKE* is determined over the entire transect. The sensitivity test is also performed on temperature, which just uses transect average temperatures. This requires slightly altering the methodology, so that all transect-scaled quantities are simply collected from all the heterogeneous and homogeneous transects to produce normalized frequency distributions. Although this methodology does not weight results from all cloud phase normalized frequencies equally (omitting the averaging in Steps 2&3 of the methodology in Section 3.4), the major trends are still observed: no discernable difference is

https://doi.org/10.5194/egusphere-2026-6201
Preprint. Discussion started: 3 November 2026
© Author(s) 2026. CC BY 4.0 License.

observed in *TKE* for heterogeneous and homogeneous transects, whereas spatially heterogeneous (homogeneous) transects occur more frequently at -10° to -5°C (-20° to -15°C).

4 Discussion

4.1 Implications of heterogeneous/homogeneous MPC differences

The aforementioned signals contrasting heterogeneous and homogeneous MPCs are plausibly linked to their temporal evolution, where more heterogeneous liquid-dominated MPCs may be indicative of the early stages of primary ice nucleation; and in contrast, spatially homogeneous liquid phase regions would indicate an absence of nearby ice and recent glaciation events. If this is the case, the heterogeneous liquid-dominated MPCs possessing higher concentrations of large drops (D~25–60 μm; Figure 9D), would suggest ice nucleation within the MPC is significantly related to the presence of large drops. This is consistent with broader drop size distributions observed for liquid-dominated MPCs compared with liquid-only clouds (Figure 8G); and is further suggested by the fact that this signal is limited to transects composed primarily of liquid phase samples (mixed phase norm. freq. < 0.5; Figure 9E), which are more likely freshly nucleated MPCs compared with transects having mostly mixed phase samples. There is much literature highlighting greater likelihoods of ice nucleation for large drops (Lamb and Verlinde, 2011; Young, 1974), which is supported by observational evidence (e.g., Coopman et al., 2020; Rangno and Hobbs, 1991). Additionally, the presence of homogeneous mixed phase regions are plausibly regions having undergone significant mixing. The greater concentrations of larger ice particles (D > 1 mm) in Figure 10A&C may be indicative of greater growth durations, possibly including significant riming.

Heterogeneous transects were also found to occur more frequently at -10° to -5°C (Figure 11B). This finding, in combination with significantly higher concentrations of large drops (D~25–60 μm) within these transects, as well as the insensitivity of heterogeneity to turbulent motion (Figure 11A), may suggest ice nucleation events are primarily contributing to the spatial heterogeneity. This is because increased turbulent motion is expected to be indirectly related to increased rates of varying secondary ice production mechanisms: such as increasing the collision rate of ice crystals associated with ice-ice collisional breakup (Takahashi et al., 1995; Vardiman, 1978), or other mechanisms such as INP activation in transient supersaturations around supercooled droplets (Korolev and Leisner, 2020). However, little work has been done to correlate turbulent motion with secondary ice production, and previous literature has also found an absence of strong correlations between the two (e.g., Heymsfield and Willis, 2014).

Increased spatial heterogeneity can arise from alternative factors as well (e.g., ice precipitating out of an MPC). Therefore, it is crucial that future research incorporate modeling and/or backtrack trajectories to consider the temporal evolution of MPCs and their phase spatial heterogeneity. For example, consider a plausible evolutionary timeline of phase heterogeneity for a liquid-dominated MPC: Initial ice nucleation events occur within a liquid-only cloud, increasing the spatial variability of ice mixed within liquid-only clouds. Subsequent mixing (perhaps including additional ice production) acts to re-homogenize the

https://doi.org/10.5194/egusphere-2026-6201
Preprint. Discussion started: 3 November 2026
© Author(s) 2026. CC BY 4.0 License.

cloud as mixed phase. Following glaciation and subsequent mixing, ice precipitation reintroduces heterogeneity due to the removal of ice crystals, which finally re-homogenizes the cloud back to a liquid-only cloud once all the ice has been removed. This scenario results in a state-switching oscillation of cloud phase spatial heterogeneity as: homogeneous→heterogeneous→homogeneous→heterogeneous→homogenous. This and other plausible pathways result in cloud evolution overlap between the heterogeneous/homogeneous statistics presented here; and must be considered in order to infer the temporal evolution of MPCs and their phase spatial variability.

Additionally, future work should relate one-dimensional measurements of ubiquitous liquid- and ice-dominated MPCs to macroscale MPC structures beyond evaluating their height statistics (Section 3.3). As previously discussed in Section 1, much literature has established the canonical three-dimensional structure of polar MPCs, whereby a layer of supercooled liquid overlies a region of precipitating ice (Boer et al., 2009; Korolev et al., 2017; Morrison et al., 2012; Shupe et al., 2006), the common occurrence of multi-layered cloud regimes (D'Alessandro et al., 2023; Shupe, 2011; Shupe et al., 2006; Verlinde et al., 2013), as well as MPCs containing layers of supercooled liquid embedded within layers of ice (Luke et al., 2010; Verlinde et al., 2013). Moreover, localized variability exists within cloud regimes such as horizontal spatial variability in cloud phase (discussed here and references within), and generating ice cells (Wang et al., 2020). Relating in situ measurements to macroscale features of MPCs and their varying structures will help contextualize findings.

4.2 Additional discussion concerning cloud phase methodology comparisons

An additional component of this study was comparing multiple cloud phase classification methodologies. These methodologies were shown to produce notably different outputs in Section 3.1, warranting future intercomparisons. A popular method not explored here relies on measurements from the hotwire Nevzorov probe. This instrument acquires measurements of *LWC* and *TWC*, and classifies liquid, ice and mixed phase samples to those having $LWC/TWC>0.9$, $LWC/TWC<0.1$ and $0.1<LWC/TWC<0.9$, respectively (e.g., Evans et al., 2025; Korolev and Milbrandt, 2022; Korolev et al., 2003; Korolev and Isaac, 2006; Lucke et al., 2024). Efforts were made to include a similar cloud phase analysis using the Nevzorov probe measurements, since it was deployed for MOSAiC-ACA and HALO-AC3. However, results are highly sensitive to the post processing of the probe, which includes accounting for collision and collection efficiencies, and the differences in the required heating of the liquid and ice particles (not shown). This is partly why previous studies include quality control for the Nevzorov probe measurements by validating the presence of liquid or ice particles with vibrating icing rod, spectrometer and/or optical imaging probe measurements (Cober et al., 2001; Korolev and Milbrandt, 2022; Korolev and Isaac, 2006). Additionally, collection efficiencies are improved by the usage of a deeper cone (12 mm depth), and this component of the probe did not properly function during MOSAiC-ACA. For these reasons, a similar analysis has been omitted. Details of the data processing and Nevzorov probe used for these campaigns can be found in Lucke (2024) and Lucke et al. (2024).

https://doi.org/10.5194/egusphere-2026-6201
Preprint. Discussion started: 3 November 2026
© Author(s) 2026. CC BY 4.0 License.

Differences were also shown in the cloud phase heterogeneity in Section 3.2 when considering a threshold of *LWC*/*TWC*=0.9 for distinguishing liquid versus mixed phase samples (Figure 5 versus Figure S3), as discussed in the previous paragraph. This poses the deeper philosophical question of *how* a mixed phase sample should be classified, beyond simply considering whether liquid and ice particles coexist in the same volume. The 0.1 and 0.9 thresholds commonly used to classify cloud phase were determined in large part to account for measurement uncertainties of the Nevzorov probe (Korolev et al., 2003). However, studies not using the Nevzorov probe commonly classify cloud phase using similar thresholds on *LWC* and *TWC* derived from alternative cloud instrumentation (e.g., D'Alessandro et al., 2019; Dammann et al., 2025; Huang et al., 2021; Yang et al., 2024). No attempt is made here to argue whether the mixed phase should be classified by just the presence of both liquid and ice, or whether some "significant" content threshold of both should be exceeded. Future work should consider this question given several underling contexts, including whether a "benchmark" classification should be an agreed upon condition, or whether differing classification methods are more suitable for differing research questions (what amount of ice and/or liquid impacts relevant process-rates, or what amounts are detectable via remote sensing retrievals, etc.).

5 Concluding remarks

The purpose of this study is to evaluate MPC characteristics over the Arctic Ocean using ~25 hours of in-cloud, in situ measurements acquired during three field campaigns based out of Svalbard, Norway. Cloud samples are reported at 1 Hz and are classified as liquid, ice or mixed phase using a novel methodology; which incorporates measurements from the Polar Nephelometer and a "semi-supervised" Bayesian Gaussian Mixture Model. This method allows for phase classification by diagnosing modes observed in seven parameters (derived from cloud particle size distributions) possessing multimodal distributions as being associated with a given cloud phase.

Additionally, we introduce three MPC types which are determined for regions of continuous in-cloud measurements: a) liquid-dominated MPCs (composed entirely of liquid droplets and patches of inter-mixed ice crystals), b) ice-dominated MPCs (composed entirely of ice crystals and patches of inter-mixed liquid droplets) and c) phase-segregated MPCs (containing liquid-only and ice-only samples). These MPC types aid in comparisons between spatially heterogeneous and spatially homogeneous MPCs by removing potential biases resulting from differences in cloud phase occurrence frequencies (Section 3.4).

We summarize our findings below:

1. Cloud phase frequencies and particle size distributions from the proposed phase classification methodology are compared with those of previous classification methodologies. Results can vary considerably amongst the methodologies—highlighting the importance of future intercomparisons between phase classification products. Our

https://doi.org/10.5194/egusphere-2026-6201
Preprint. Discussion started: 3 November 2026
© Author(s) 2026. CC BY 4.0 License.

approach captures expected differences in PSD shapes, produces reasonable phase frequency distributions, and avoids the inclusion of excessively large particles in liquid phase samples (diameters exceeding ~1 mm).

2. Liquid-phase samples within liquid-dominated MPCs have broader PSDs than those in liquid-only clouds, and also possess greater concentrations of small droplets (diameters < 10 μm). Ice phase samples within ice-dominated MPCs have greater ice concentrations compared with those in ice-only clouds. Mixed phase samples within liquid-dominated MPCs have greater (lower) concentrations of liquid (ice) particles having diameters ~6–100 μm (>100 μm) compared with ice-dominated MPCs.
3. Spatially heterogeneous liquid-dominated MPCs have higher (lower) concentrations of large droplets having diameters ~25–60 μm (ice crystals having diameters>1000 μm) than spatially homogeneous MPCs. Spatially heterogeneous ice-dominated clouds have higher concentrations of small ice (diameters less than 100 μm) compared with spatially homogeneous MPCs.
4. Spatially heterogeneous (homogeneous) liquid-dominated MPCs occur more frequently at approximately -10° to -5°C (-20° to -15°C), whereas no major differences are observed in turbulent kinetic energy.

This study highlights the advantage of discretizing MPCs into three separate categories, which may help elucidate relevant mechanisms and coupled-processes at varying spatial scales. For example, by only considering two phase classifications rather than three (i.e., liquid, ice and mixed phase) in liquid- and ice-dominated MPCs, an analysis of cloud phase spatial heterogeneity is possible by controlling for differences in the occurrence frequencies of different cloud phases (by only accounting for two cloud phase categories, rather than three). This was done in our study, allowing for the first comparison of heterogeneous and homogeneous MPCs which are not biased by differences in cloud phase occurrence frequencies. We recommend future work relate these MPCs types as well as spatially heterogeneity statistics to lifetimes and temporal evolution of MPCs, where potential pathways may exist within certain meteorological contexts (e.g., cold air outbreaks).

We previously mentioned how cloud phase classification comparisons reveal significantly diverging outputs amongst the different methodologies. Notable differences were also observed for sensitivity tests whereby a commonly used *LWC/TWC* condition (Korolev et al., 2003) is applied to the proposed methodology. Such differences, despite applying similar assumptions and only minor adjustments, suggest cloud phase classification intercomparisons are deeply warranted.

Appendix

This section introduces how the methodology in Section 3.4 is applied to PSDs within heterogeneous and homogeneous transects. Results here characterize the differences of PSDs within spatially heterogeneous and homogeneous liquid-dominated transects having 15 consecutive 1 Hz in-cloud samples (i.e., 15 seconds of continuous in-cloud measurements). Figure A1A shows averaged PSDs of the mixed phase samples (following the proposed methodology) taken from spatially homogeneous transects (red line) and heterogeneous transects (blue line). These averaged PSDs come from first separately

https://doi.org/10.5194/egusphere-2026-6201
Preprint. Discussion started: 3 November 2026
© Author(s) 2026. CC BY 4.0 License.

averaging all mixed phase PSDs from transects having identical mixed phase normalized frequencies (Step 2 in Section 3.4). Following this, these averaged PSDs from each mixed phase normalized frequency are then averaged together (Step 3 in Section 3.4). Figure A1B shows similarly averaged PSDs of the liquid phase samples. Transects are split into heterogeneous and homogeneous transects using the median SHS_{cld}, which is shown as the dotted-line in Figure A1C for each mixed phase normalized frequency (x-axis), where spatially homogeneous (heterogeneous) clouds have SHS_{cld} greater (lower) than this value. The solid line shows the total number of transects obtained at each mixed phase normalized frequency, where approximately half of the transects at each normalized frequency will correspond to the number of heterogeneous and homogeneous transects.

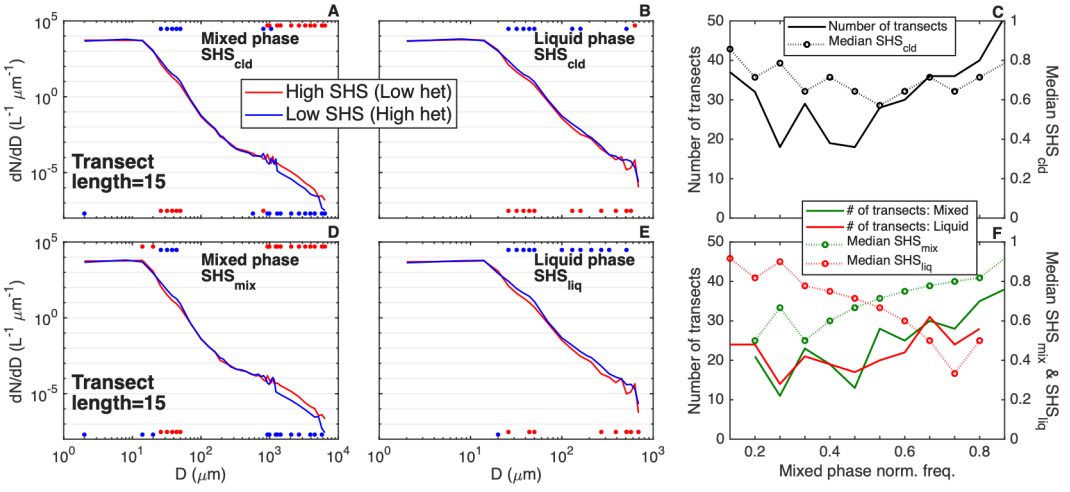


Figure A1: Characterizing differences in PSDs between spatially heterogeneous and homogeneous liquid-dominated transects (blue and red lines, respectively). Differences between heterogeneous and homogeneous transects are shown for the mixed phase A) and liquid phase B) when computing heterogeneity over the entire cloud (SHS_{cld}), as well as for measures of heterogeneity of the respective phases (SHS_{mix} and SHS_{liq}) in D) and E). C) The number of transects (solid lines) available from each combination of mixed and liquid phase occurrence frequencies (shown as the ratio of the number of mixed phase samples over the number of liquid and mixed phase samples; i.e., mixed phase normalized frequency), as well as the median SHS_{cld} for each mixed phase normalized frequency (dotted line) used in A&B. F) Identical to C but shown for the respective phases used in D&E. Particle concentration bins with significantly high or low concentrations are denoted by the shaded circles, colored accordingly to transect SHS (the method to determine significance is provided in the text). The transect length (i.e., number of consecutive in-cloud samples) is 15 seconds. Results are restricted to temperatures from -20°–0°C.

Differences are observed in the mixed phase PSDs between the spatially heterogeneous and homogeneous transects. Namely, there are more particles having D from ~25–50 µm in spatially heterogeneous transects, which is similarly observed for the

https://doi.org/10.5194/egusphere-2026-6201
Preprint. Discussion started: 3 November 2026
© Author(s) 2026. CC BY 4.0 License.

liquid phase in A1B. There are also fewer particles having D>900 µm in spatially heterogeneous transects, which can be confidently diagnosed as ice crystals (e.g., looking at particle imagery). These two trends are statistically significant, as denoted by the overlying and underlying shaded circles. Specifically, the shaded circles within each panel correspond to particle concentrations which are significantly greater (circles near the upper abscissa) or lower (circles near the lower abscissa) than the population of transects. Significance is determined using a permutation method, where the same methodology used here is repeated 10,000 times; except the same number of transects as the high and low *SHS* transects are randomly selected at each mixed phase normalized frequency. The actual PSDs are then compared with the 10,000 simulated PSDs, and if concentrations in a given bin exceed those from 90% of the simulated PSDs, or are less than 10% of those from the simulated PSDs, then they are deemed significantly high or low concentrations, respectively.

The results in Figure A1A–C quantify the "absolute" heterogeneity of transects (using SHS_{cld}). However, the heterogeneity of mixed and liquid phase samples are not necessarily inversely related to each other. Because of this, Figure A1D–F uses separate measures of heterogeneity for mixed and liquid phase samples (SHS_{mix} and SHS_{liq}, respectively). Note that the aforementioned trends are all similarly observed here. Figure A1F shows the median SHS_{liq} and SHS_{mix}, where the respective heterogeneity measures decrease with a decreasing number of samples. Note that this is not indicative of an absolute change in heterogeneity of the respective phases with decreasing samples, but rather occurs as a consequence of limiting the number of samples. This was tested by simulating a 2-dimensional cloud with varying spatial heterogeneities and "sampling" the cloud by simulating linear trajectories through it (not shown).

Differences in the PSDs in Figure A1A,B,D,E are difficult to discern due to the panel log-scaling of the y-axis. To better depict differences, Figure 9 in Section 3.4 shows the ratios of PSDs from the heterogeneous transects over those from homogeneous transects (red lines). Significance is tested slightly differently than for PSDs in Figure A1A. Instead of determining whether bin concentrations are significantly high or low, the ratios of the bin concentrations are tested for significance by computing the ratios for 10,000 permutations. The actual ratios exceeding 90% of the simulated ratios tells us that the heterogeneous concentrations are significantly greater than the homogeneous concentrations. If the actual ratios are less than those of 10% of the simulated ratios, this tells us that the heterogeneous concentrations are significantly lower than the homogeneous concentrations.

Code and Data Availability Statement

In situ cloud microphysical data (CDP, CAS, 2D-S, CIP, and PIP) from the AFLUX, MOSAiC-ACA, and HALO-(AC)^3 campaigns are freely available from the World Data Center PANGAEA: https://doi.org/10.1594/PANGAEA.940564 (Moser and Voigt, 2022); https://doi.org/10.1594/PANGAEA.940557 (Moser et al., 2022);

https://doi.org/10.5194/egusphere-2026-6201
Preprint. Discussion started: 3 November 2026
© Author(s) 2026. CC BY 4.0 License.

https://doi.org/10.1594/PANGAEA.963247840 (Moser et al., 2023a); https://doi.org/10.1594/PANGAEA.941498 (Dupuy et al., 2022a); https://doi.org/10.1594/PANGAEA.941538 (Dupuy et al., 2022b); https://doi.org/10.1594/PANGAEA.965734 (Dupuy et al., 2024). Code is available upon request.

Acknowledgements

We thank all those who gathered, worked with, and provided data from the AFLUX, MOSAiC-ACA and HALO-AC3 field campaigns. The authors are grateful to the AWI for providing and operating the two Polar 5 and Polar 6 aircraft via grant numbers AWI_PA_02087, AWI_PA_02107, AWI_PA_02112, and AWI_PA_02126. We also acknowledge the funding by the Deutsche Forschungsgemeinschaft (DFG, German Research Foundation) within the framework of the Transregional Collaborative Research Center (TRR 172) "ArctiC Amplification: Climate Relevant Atmospheric and SurfaCe Processes and Feedback Mechanisms (AC)3 ". John D'Alessandro and Odran Sourdeval were supported by ANR and DFG (grant no. ANR-23-CE01-0022) for project GLACIATE; Odran Sourdeval acknowledges support by the Simons Foundation (grant no. SFI-MPS-SRM-00012102) and the Centre National d'Etudes Spatiales (CNES) through the EarthCARE and CIRSys3D projects. This work is a contribution to the $(MPC)^2$ project supported by the French Agence Nationale de la Recherche under the grant ANR-22-CE01-0009 and involving Olivier Jourdan, Guillaume Mioche, Odran Sourdeval, Aymeric Dziduch and Antoine Baudoux. We also acknowledge the funding by the Deutsche Forschungsgemeinschaft (DFG, German Research Foundation) within the framework of the Transregional Collaborative Research Center (TRR 172) "ArctiC Amplification: Climate Relevant Atmospheric and SurfaCe Processes and Feedback Mechanisms $(AC)^3$ ".

Competing Interests

The authors declare that they have no conflict of interest.

Author Contributions

J.D. designed the research methodology and performed the data analysis, with significant contributions from the coauthors.

References

Bergeron, T.: On the physics of clouds and precipitation, Proces Verbaux de l'Association de Météorologie, International Union of Geodesy and Geophysics, 156–178, 1935.

Bertrand, L., Kay, J. E., and de Boer, G.: Increasing wintertime cloud opacity increases surface longwave radiation at a long-term Arctic observatory, Nat Commun, 16, 9135, https://doi.org/10.1038/s41467-025-64441-8, 2025.

Boer, G. de, Eloranta, E. W., and Shupe, M. D.: Arctic Mixed-Phase Stratiform Cloud Properties from Multiple Years of Surface-Based Measurements at Two High-Latitude Locations, Journal of the Atmospheric Sciences, 66, 2874–2887, https://doi.org/10.1175/2009JAS3029.1, 2009.

https://doi.org/10.5194/egusphere-2026-6201
Preprint. Discussion started: 3 November 2026
© Author(s) 2026. CC BY 4.0 License.

Cesana, G. and Storelvmo, T.: Improving climate projections by understanding how cloud phase affects radiation, Journal of Geophysical Research: Atmospheres, 122, 4594–4599, https://doi.org/10.1002/2017JD026927, 2017.

Cober, S. G., Isaac, G. A., Korolev, A. V., and Strapp, J. W.: Assessing Cloud-Phase Conditions, Journal of Applied Meteorology, 40, 1967–1983, https://doi.org/10.1175/1520-0450(2001)040%3C1967:ACPC%3E2.0.CO;2, 2001.

Coopman, Q. and Tan, I.: Characterization of the Spatial Distribution of the Thermodynamic Phase Within Mixed-Phase Clouds Using Satellite Observations, Geophysical Research Letters, 50, e2023GL104977, https://doi.org/10.1029/2023GL104977, 2023.

Coopman, Q., Hoose, C., and Stengel, M.: Analysis of the Thermodynamic Phase Transition of Tracked Convective Clouds Based on Geostationary Satellite Observations, Journal of Geophysical Research: Atmospheres, 125, e2019JD032146, https://doi.org/10.1029/2019JD032146, 2020.

Costa, A., Meyer, J., Afchine, A., Luebke, A., Günther, G., Dorsey, J. R., Gallagher, M. W., Ehrlich, A., Wendisch, M., Baumgardner, D., Wex, H., and Krämer, M.: Classification of Arctic, midlatitude and tropical clouds in the mixed-phase temperature regime, Atmospheric Chemistry and Physics, 17, 12219–12238, https://doi.org/10.5194/acp-17-12219-2017, 2017.

Crosier, J., Bower, K. N., Choularton, T. W., Westbrook, C. D., Connolly, P. J., Cui, Z. Q., Crawford, I. P., Capes, G. L., Coe, H., Dorsey, J. R., Williams, P. I., Illingworth, A. J., Gallagher, M. W., and Blyth, A. M.: Observations of ice multiplication in a weakly convective cell embedded in supercooled mid-level stratus, Atmospheric Chemistry and Physics, 11, 257–273, https://doi.org/10.5194/acp-11-257-2011, 2011.

D'Alessandro, J., Sourdeval, O., and Krämer, M.: Spatial Heterogeneity and Inhomogeneity of Cirrus Microphysical Properties on Kilometer Spatial Scales, Geophysical Research Letters, 53, e2026GL122025, https://doi.org/10.1029/2026GL122025, 2026.

D'Alessandro, J. J., Diao, M., Wu, C., Liu, X., Jensen, J. B., and Stephens, B. B.: Cloud phase and relative humidity distributions over the Southern Ocean in austral summer based on in situ observations and CAM5 simulations, Journal of Climate, 32, 2781–2805, https://doi.org/10.1175/JCLI-D-18-0232.1, 2019.

D'Alessandro, J. J., McFarquhar, G. M., Wu, W., Stith, J. L., Jensen, J. B., and Rauber, R. M.: Characterizing the Occurrence and Spatial Heterogeneity of Liquid, Ice, and Mixed Phase Low-Level Clouds Over the Southern Ocean Using in Situ Observations Acquired During SOCRATES, Journal of Geophysical Research: Atmospheres, 126, e2020JD034482, https://doi.org/10.1029/2020JD034482, 2021.

D'Alessandro, J. J., Mcfarquhar, G. M., Stith, J. L., Jensen, J. B., Diao, Minghui., DeMott, P. J., and Sanchez, K. J.: An evaluation of phase, aerosol-cloud interactions and microphysical properties of single- and multi-layer clouds over the Southern Ocean using in situ observations from SOCRATES, Journal of Geophysical Research: Atmospheres, https://doi.org/10.1029/2023JD038610, 2023.

D'Alessandro, J. J., Wood, R., and Blossey, P. N.: Evaluating Entrainment–Mixing Characteristics through Direct Comparisons of Drop Size Distributions Using In Situ Observations from ACE-ENA, Journal of the Atmospheric Sciences, 82, 2521–2540, https://doi.org/10.1175/JAS-D-24-0153.1, 2025.

Dammann, S. L.-S., Schäfer, B., David, R. O., and Storelvmo, T.: Observations and Model Simulations of Phase Heterogeneity in Arctic Clouds, Journal of Geophysical Research: Atmospheres, 130, e2024JD042714, https://doi.org/10.1029/2024JD042714, 2025.

https://doi.org/10.5194/egusphere-2026-6201
Preprint. Discussion started: 3 November 2026
© Author(s) 2026. CC BY 4.0 License.

Deng, Y., Yang, J., Yin, Y., Lu, C., Chen, B., Dong, X., Wang, Z., Zhang, B., Bao, X., and Hou, T.: On the Relationship Between Condensed Water Content and Liquid-Ice Mixing Homogeneity in Mixed-Phase Stratiform Clouds, Geophysical Research Letters, 51, e2024GL110670, https://doi.org/10.1029/2024GL110670, 2024.

Druckenmiller, M. L., Thoman, R. L., Moon, T. A., and Eds.: Arctic Report Card 2025, https://doi.org/https://doi.org/10.25923/nrzf-j897, 2025.

Dziduch, A., Baudoux, A., Mioche, G., Canzi, A., Doiteau, B., Moser, M., Järvinen, E., Vignon, É., Raut, J.-C., Dupuy, R., Gourbeyre, C., Baray, J.-L., Monier, M., Szczap, F., Penide, G., Delanoë, J., Sourdeval, O., Schwarzenboeck, A., Mertes, S., Schnaiter, F. M., Voigt, C., Mech, M., Crewell, S., Herber, A., Lüpkes, C., Ehrlich, A., Wendisch, M., and Jourdan, O.: Microphysical Properties and Ice Crystal Habits of Low-Level Arctic Mixed-Phase Clouds from Four Airborne In Situ Campaigns over the Svalbard Seas, EGUsphere, 1–49, https://doi.org/10.5194/egusphere-2026-3265, 2026a.

Dziduch, A., Mioche, G., Coopman, Q., Bazantay, C., Delanoë, J., and Jourdan, O.: Regional and seasonal distribution of Arctic low-level cloud types and their relationship to large-scale environmental conditions, Atmospheric Chemistry and Physics, 26, 4019–4047, https://doi.org/10.5194/acp-26-4019-2026, 2026b.

Ehrlich, A., Wendisch, M., Lüpkes, C., Buschmann, M., Bozem, H., Chechin, D., Clemen, H.-C., Dupuy, R., Eppers, O., Hartmann, J., Herber, A., Jäkel, E., Järvinen, E., Jourdan, O., Kästner, U., Kliesch, L.-L., Köllner, F., Mech, M., Mertes, S., Neuber, R., Ruiz-Donoso, E., Schnaiter, M., Schneider, J., Stapf, J., and Zanatta, M.: A comprehensive in situ and remote sensing data set from the Arctic CLoud Observations Using airborne measurements during polar Day (ACLOUD) campaign, Earth System Science Data, 11, 1853–1881, https://doi.org/10.5194/essd-11-1853-2019, 2019.

Ehrlich, A., Crewell, S., Herber, A., Klingebiel, M., Lüpkes, C., Mech, M., Becker, S., Borrmann, S., Bozem, H., Buschmann, M., Clemen, H.-C., De La Torre Castro, E., Dorff, H., Dupuy, R., Eppers, O., Ewald, F., George, G., Giez, A., Grawe, S., Gourbeyre, C., Hartmann, J., Jäkel, E., Joppe, P., Jourdan, O., Jurányi, Z., Kirbus, B., Lucke, J., Luebke, A. E., Maahn, M., Maherndl, N., Mallaun, C., Mayer, J., Mertes, S., Mioche, G., Moser, M., Müller, H., Pörtge, V., Risse, N., Roberts, G., Rosenburg, S., Röttenbacher, J., Schäfer, M., Schaefer, J., Schäfler, A., Schirmacher, I., Schneider, J., Schnitt, S., Stratmann, F., Tatzelt, C., Voigt, C., Walbröl, A., Weber, A., Wetzel, B., Wirth, M., and Wendisch, M.: A comprehensive in situ and remote sensing data set collected during the HALO–($\mathcal{AC}$)^3 aircraft campaign, Earth System Science Data, 17, 1295–1328, https://doi.org/10.5194/essd-17-1295-2025, 2025.

Esselborn, M., Wirth, M., Fix, A., Tesche, M., and Ehret, G.: Airborne high spectral resolution lidar for measuring aerosol extinction and backscatter coefficients, Applied Optics, 47, 346–358, https://doi.org/10.1364/AO.47.000346, 2008.

Evans, M. D., Abel, S. J., Field, P. R., Finney, D. L., Lloyd, G., Cotton, R. J., Smith, D. K. E., Murray, B. J., and Huang, X.: Characterising the spatial overlap between liquid and ice in mixed-phase clouds, Quarterly Journal of the Royal Meteorological Society, 151, e5041, https://doi.org/10.1002/qj.5041, 2025.

Findeisen, W.: Kolloid-meteorologische Vorgänge bei Neiderschlags-bildung, Meteorologische Zeitschrift, 55, 121–133, 1938.

Finlon, J. A., McFarquhar, G. M., Nesbitt, S. W., Rauber, R. M., Morrison, H., Wu, W., and Zhang, P.: A novel approach for characterizing the variability in mass–dimension relationships: results from MC3E, Atmospheric Chemistry and Physics, 19, 3621–3643, https://doi.org/10.5194/acp-19-3621-2019, 2019.

Gayet, J. F., Crépel, O., Fournol, J. F., and Oshchepkov, S.: A new airborne polar Nephelometer for the measurements of optical and microphysical cloud properties. Part I: Theoretical design, Annales Geophysicae, 15, 451–459, https://doi.org/10.1007/s00585-997-0451-1, 1997.

https://doi.org/10.5194/egusphere-2026-6201
Preprint. Discussion started: 3 November 2026
© Author(s) 2026. CC BY 4.0 License.

Hartmann, J., Gehrmann, M., Kohnert, K., Metzger, S., and Sachs, T.: New calibration procedures for airborne turbulence measurements and accuracy of the methane fluxes during the AirMeth campaigns, Atmospheric Measurement Techniques, 11, 4567–4581, https://doi.org/10.5194/amt-11-4567-2018, 2018.

Heymsfield, A. and Willis, P.: Cloud Conditions Favoring Secondary Ice Particle Production in Tropical Maritime Convection, Journal of the Atmospheric Sciences, 71, 4500–4526, https://doi.org/10.1175/JAS-D-14-0093.1, 2014.

Heymsfield, A. J., Field, P. R., Bailey, M., Rogers, D., Stith, J., Twohy, C., Wang, Z., and Haimov, S.: Ice in clouds experiment-layer clouds. Part I: Ice growth rates derived from lenticular wave cloud penetrations, Journal of the Atmospheric Sciences, 68, 2628–2654, https://doi.org/10.1175/JAS-D-11-025.1, 2011.

Hogan, R. J., Tian, L., Brown, P. R. A., Westbrook, C. D., Heymsfield, A. J., and Eastment, J. D.: Radar Scattering from Ice Aggregates Using the Horizontally Aligned Oblate Spheroid Approximation, Journal of Applied Meteorology and Climatology, 51, 655–671, https://doi.org/10.1175/JAMC-D-11-074.1, 2012.

Huang, Y., Siems, S. T., and Manton, M. J.: Wintertime In Situ Cloud Microphysical Properties of Mixed-Phase Clouds Over the Southern Ocean, Journal of Geophysical Research: Atmospheres, 126, e2021JD034832, https://doi.org/10.1029/2021JD034832, 2021.

Jourdan, O., Mioche, G., Garrett, T. J., Schwarzenböck, A., Vidot, J., Xie, Y., Shcherbakov, V., Yang, P., and Gayet, J.-F.: Coupling of the microphysical and optical properties of an Arctic nimbostratus cloud during the ASTAR 2004 experiment: Implications for light-scattering modeling, Journal of Geophysical Research: Atmospheres, 115, https://doi.org/10.1029/2010JD014016, 2010.

Kanji, Z. A., Ladino, L. A., Wex, H., Boose, Y., Burkert-Kohn, M., Cziczo, D. J., and Krämer, M.: Overview of Ice Nucleating Particles, Meteorological Monographs, 58, 1.1-1.33, https://doi.org/10.1175/AMSMONOGRAPHS-D-16-0006.1, 2017.

Kirschler, S., Voigt, C., Anderson, B. E., Chen, G., Crosbie, E. C., Ferrare, R. A., Hahn, V., Hair, J. W., Kaufmann, S., Moore, R. H., Painemal, D., Robinson, C. E., Sanchez, K. J., Scarino, A. J., Shingler, T. J., Shook, M. A., Thornhill, K. L., Winstead, E. L., Ziemba, L. D., and Sorooshian, A.: Overview and statistical analysis of boundary layer clouds and precipitation over the western North Atlantic Ocean, Atmospheric Chemistry and Physics, 23, 10731–10750, https://doi.org/10.5194/acp-23-10731-2023, 2023.

Kolmogorov, A. N.: The local structure of turbulence in incompressible viscous fluid for very large Reynolds numbers, Proceedings of the Royal Society of London. Series A: Mathematical and Physical Sciences, 434, 9–13, https://doi.org/10.1098/rspa.1991.0075, 1991.

Korolev, A. and Field, P. R.: The Effect of Dynamics on Mixed-Phase Clouds: Theoretical Considerations, Journal of the Atmospheric Sciences, 65, 66–86, https://doi.org/10.1175/2007JAS2355.1, 2008.

Korolev, A. and Leisner, T.: Review of experimental studies of secondary ice production, Atmospheric Chemistry and Physics, 20, 11767–11797, https://doi.org/10.5194/acp-20-11767-2020, 2020.

Korolev, A. and Milbrandt, J.: How Are Mixed-Phase Clouds Mixed?, Geophysical Research Letters, 49, e2022GL099578, https://doi.org/10.1029/2022GL099578, 2022.

Korolev, A., McFarquhar, G., Field, P. R., Franklin, C., Lawson, P., Wang, Z., Williams, E., Abel, S. J., Axisa, D., Borrmann, S., Crosier, J., Fugal, J., Krämer, M., Lohmann, U., Schlenczek, O., Schnaiter, M., and Wendisch, M.: Mixed-

© Author(s) 2026. CC BY 4.0 License.

Phase Clouds: Progress and Challenges, Meteorological Monographs, 58, 5.1-5.50, https://doi.org/10.1175/AMSMONOGRAPHS-D-17-0001.1, 2017.

Korolev, A. V. and Isaac, G. A.: Relative Humidity in Liquid, Mixed-Phase, and Ice Clouds, Journal of the Atmospheric Sciences, 63, 2865–2880, https://doi.org/10.1175/JAS3784.1, 2006.

Korolev, A. V., Isaac, G. A., Cober, S. G., Strapp, J. W., and Hallett, J.: Microphysical characterization of mixed-phase clouds, Quarterly Journal of the Royal Meteorological Society, 129, 39–65, https://doi.org/10.1256/qj.01.204, 2003.

Lamb, D. and Verlinde, J.: Physics and chemistry of clouds, Cambridge University Press, 1–584 pp., https://doi.org/10.1017/CBO9780511976377, 2011.

Lance, S., Brock, C. A., Rogers, D., and Gordon, J. A.: Water droplet calibration of the Cloud Droplet Probe (CDP) and in-flight performance in liquid, ice and mixed-phase clouds during ARCPAC, Atmospheric Measurement Techniques, 3, 1683–1706, https://doi.org/10.5194/amt-3-1683-2010, 2010.

Lucke, J.: Detection and differentiation of supercooled large droplet icing conditions, thesis, Delft University of Technology, 196 pp., 2024.

Lucke, J. R., Jurkat, T., Baumgardner, D., Kalinka, F., Moser, M., Castro, E. D. L. T., and Voigt, C.: Characterization of Atmospheric Icing Conditions during the HALO-(AC) ^{3} Campaign with the Nevzorov Probe and the Backscatter Cloud Probe with Polarization Detection, SAE International Journal of Advances and Current Practices in Mobility, 6, 1224–1237, https://doi.org/10.4271/2023-01-1485, 2024.

Luke, E. P., Kollias, P., and Shupe, M. D.: Detection of supercooled liquid in mixed-phase clouds using radar Doppler spectra, Journal of Geophysical Research: Atmospheres, 115, https://doi.org/10.1029/2009JD012884, 2010.

Matus, A. V. and L'Ecuyer, T. S.: The role of cloud phase in Earth's radiation budget, Journal of Geophysical Research: Atmospheres, 122, 2559–2578, https://doi.org/10.1002/2016JD025951, 2017.

McFarquhar, G., Zhang, G., Poellot, M. R., Kok, G. L., McCoy, R., Tooman, T., Fridlind, A., and Heymsfield, A. J.: Ice properties of single-layer stratocumulus during the Mixed-Phase Arctic Cloud Experiment: 1. Observations, Journal of Geophysical Research, 112, D24201, https://doi.org/10.1029/2007JD008633, 2007.

McFarquhar, G. M. and Cober, S. G.: Single-scattering properties of mixed-phase Arctic clouds at solar wavelengths: Impacts on radiative transfer, Journal of Climate, 17, 3799–3813, https://doi.org/10.1175/1520-0442(2004)017%3C3799:SPOMAC%3E2.0.CO;2, 2004.

Mech, M., Ehrlich, A., Herber, A., Lüpkes, C., Wendisch, M., Becker, S., Boose, Y., Chechin, D., Crewell, S., Dupuy, R., Gourbeyre, C., Hartmann, J., Jäkel, E., Jourdan, O., Kliesch, L.-L., Klingebiel, M., Kulla, B. S., Mioche, G., Moser, M., Risse, N., Ruiz-Donoso, E., Schäfer, M., Stapf, J., and Voigt, C.: MOSAiC-ACA and AFLUX - Arctic airborne campaigns characterizing the exit area of MOSAiC, Sci Data, 9, 790, https://doi.org/10.1038/s41597-022-01900-7, 2022.

Mioche, G., Jourdan, O., Ceccaldi, M., and Delanoë, J.: Variability of mixed-phase clouds in the Arctic with a focus on the Svalbard region: A study based on spaceborne active remote sensing, Atmospheric Chemistry and Physics, 15, 2445–2461, https://doi.org/10.5194/acp-15-2445-2015, 2015.

Mioche, G., Jourdan, O., Delanoë, J., Gourbeyre, C., Febvre, G., Dupuy, R., Monier, M., Szczap, F., Schwarzenboeck, A., and Gayet, J. F.: Vertical distribution of microphysical properties of Arctic springtime low-level mixed-phase clouds over

© Author(s) 2026. CC BY 4.0 License.

the Greenland and Norwegian seas, Atmospheric Chemistry and Physics, 17, 12845–12869, https://doi.org/10.5194/acp-17-12845-2017, 2017.

Morrison, H., de Boer, G., Feingold, G., Harrington, J., Shupe, M. D., and Sulia, K.: Resilience of persistent Arctic mixed-phase clouds, Nature Geoscience, 5, 11–17, https://doi.org/10.1038/ngeo1332, 2012.

Moser, M., Voigt, C., Jurkat-Witschas, T., Hahn, V., Mioche, G., Jourdan, O., Dupuy, R., Gourbeyre, C., Schwarzenboeck, A., Lucke, J., Boose, Y., Mech, M., Borrmann, S., Ehrlich, A., Herber, A., Lüpkes, C., and Wendisch, M.: Microphysical and thermodynamic phase analyses of Arctic low-level clouds measured above the sea ice and the open ocean in spring and summer, Atmospheric Chemistry and Physics, 23, 7257–7280, https://doi.org/10.5194/acp-23-7257-2023, 2023.

Moser, M., Voigt, C., Eppers, O., Lucke, J., De La Torre Castro, E., Mayer, J., Dupuy, R., Mioche, G., Jourdan, O., Clemen, H.-C., Schneider, J., Joppe, P., Mertes, S., Wetzel, B., Borrmann, S., Klingebiel, M., Mech, M., Lüpkes, C., Crewell, S., Ehrlich, A., Herber, A., and Wendisch, M.: The Arctic Low-Level Mixed-Phase Haze Regime and its Microphysical Differences to Mixed-Phase Clouds, Atmospheric Chemistry and Physics, 26, 1867–1887, https://doi.org/10.5194/acp-26-1867-2026, 2026.

Rangno, A. L. and Hobbs, P. V.: Ice particle concentrations and precipitation development in small polar maritime cumuliform clouds, Quarterly Journal of the Royal Meteorological Society, 117, 207–241, https://doi.org/10.1002/qj.49711749710, 1991.

Rauber, R. M. and Tokay, A.: An Explanation for the Existence of Supercooled Water at the Top of Cold Clouds, Journal of the Atmospheric Sciences, 48, 1005–1023, https://doi.org/10.1175/1520-0469(1991)048%3C1005:AEFTEO%3E2.0.CO;2, 1991.

Ruiz-Donoso, E., Ehrlich, A., Schäfer, M., Jäkel, E., Schemann, V., Crewell, S., Mech, M., Kulla, B. S., Kliesch, L.-L., Neuber, R., and Wendisch, M.: Small-scale structure of thermodynamic phase in Arctic mixed-phase clouds observed by airborne remote sensing during a cold air outbreak and a warm air advection event, Atmospheric Chemistry and Physics, 20, 5487–5511, https://doi.org/10.5194/acp-20-5487-2020, 2020.

Schulte, L., Forbes, R., Magnusson, L., Schemann, V., Day, J., and Crewell, S.: Towards improving Arctic mixed-phase cloud representation in the ECMWF model using MOSAiC observations, Quarterly Journal of the Royal Meteorological Society, n/a, e70205, https://doi.org/10.1002/qj.70205, 2026.

Shaw, J., McGraw, Z., Bruno, O., Storelvmo, T., and Hofer, S.: Using Satellite Observations to Evaluate Model Microphysical Representation of Arctic Mixed-Phase Clouds, Geophysical Research Letters, 49, e2021GL096191, https://doi.org/10.1029/2021GL096191, 2022.

Shupe, M. D.: Clouds at arctic atmospheric observatories. Part II: Thermodynamic phase characteristics, Journal of Applied Meteorology and Climatology, 50, 645–661, https://doi.org/10.1175/2010JAMC2468.1, 2011.

Shupe, M. D., Matrosov, S. Y., and Uttal, T.: Arctic mixed-phase cloud properties derived from surface-based sensors at SHEBA, Journal of the Atmospheric Sciences, 63, 697–711, https://doi.org/10.1175/JAS3659.1, 2006.

Shupe, M. D., Kollias, P., Persson, P. O. G., and McFarquhar, G. M.: Vertical Motions in Arctic Mixed-Phase Stratiform Clouds, Journal of the Atmospheric Sciences, 65, 1304–1322, https://doi.org/10.1175/2007JAS2479.1, 2008.

Sokol, A. B. and Storelvmo, T.: The Spatial Heterogeneity of Cloud Phase Observed by Satellite, Journal of Geophysical Research: Atmospheres, 129, e2023JD039751, https://doi.org/10.1029/2023JD039751, 2024.

https://doi.org/10.5194/egusphere-2026-6201
Preprint. Discussion started: 3 November 2026
© Author(s) 2026. CC BY 4.0 License.

Sun, Z. and Shine, K. P.: Studies of the radiative properties of ice and mixed-phase clouds, Quarterly Journal of the Royal Meteorological Society, 120, 111–137, https://doi.org/10.1002/qj.49712051508, 1994.

Suzuki, K., Nagao, T. M., and Murai, A.: Satellite-Based Diagnostics of Precipitation Process in Mixed-Phase Clouds: Extension From Warm Rain Process Statistics, Geophysical Research Letters, 51, e2024GL110573, https://doi.org/10.1029/2024GL110573, 2024.

Takahashi, T., Nagao, Y., and Kushiyama, Y.: Possible High Ice Particle Production during Graupel–Graupel Collisions, Journal of the Atmospheric Sciences, 52, 4523–4527, https://doi.org/10.1175/1520-0469(1995)052%3C4523:PHIPPD%3E2.0.CO;2, 1995.

Tan, I. and Storelvmo, T.: Sensitivity Study on the Influence of Cloud Microphysical Parameters on Mixed-Phase Cloud Thermodynamic Phase Partitioning in CAM5, Journal of the Atmospheric Sciences, 73, 709–728, https://doi.org/10.1175/JAS-D-15-0152.1, 2016.

Touloupas, G., Lauber, A., Henneberger, J., Beck, A., and Lucchi, A.: A convolutional neural network for classifying cloud particles recorded by imaging probes, Atmospheric Measurement Techniques, 13, 2219–2239, https://doi.org/10.5194/amt-13-2219-2020, 2020.

Vardiman, L.: The Generation of Secondary Ice Particles in Clouds by Crystal–Crystal Collision, Journal of the Atmospheric Sciences, 35, 2168–2180, https://doi.org/10.1175/1520-0469(1978)035%3C2168:TGOSIP%3E2.0.CO;2, 1978.

Verlinde, J., Rambukkange, M. P., Clothiaux, E. E., McFarquhar, G. M., and Eloranta, E. W.: Arctic multilayered, mixed-phase cloud processes revealed in millimeter-wave cloud radar Doppler spectra, Journal of Geophysical Research: Atmospheres, 118, 13,199-13,213, https://doi.org/10.1002/2013JD020183, 2013.

Wallentin, G., Ickes, L., Achtert, P., Tesche, M., and Hoose, C.: The prevalence of Arctic multilayer clouds and their observed and modelled characteristics, Atmospheric Chemistry and Physics, 26, 3069–3089, https://doi.org/10.5194/acp-26-3069-2026, 2026.

Wang, D., Yang, C. A., and Diao, M.: Validation of Satellite-Based Cloud Phase Distributions Using Global-Scale In Situ Airborne Observations, Earth and Space Science, 11, e2023EA003355, https://doi.org/10.1029/2023EA003355, 2024.

Wang, Y., McFarquhar, G. M., Rauber, R. M., Zhao, C., Wu, W., Finlon, J. A., Stechman, D. M., Stith, J., Jensen, J. B., Schnaiter, M., Järvinen, E., Waitz, F., Vivekanandan, J., Dixon, M., Rainwater, B., and Toohey, D. W.: Microphysical Properties of Generating Cells Over the Southern Ocean: Results From SOCRATES, Journal of Geophysical Research: Atmospheres, 125, e2019JD032237, https://doi.org/10.1029/2019JD032237, 2020.

Wegener, A.: Thermodynamik der Atmosphäre, J. A. Barth, Leipzig, Germany, 1911.

Wendisch, M., Crewell, S., Ehrlich, A., Herber, A., Kirbus, B., Lüpkes, C., Mech, M., Abel, S. J., Akansu, E. F., Ament, F., Aubry, C., Becker, S., Borrmann, S., Bozem, H., Brückner, M., Clemen, H.-C., Dahlke, S., Dekoutsidis, G., Delanoë, J., De La Torre Castro, E., Dorff, H., Dupuy, R., Eppers, O., Ewald, F., George, G., Gorodetskaya, I. V., Grawe, S., Groß, S., Hartmann, J., Henning, S., Hirsch, L., Jäkel, E., Joppe, P., Jourdan, O., Jurányi, Z., Karalis, M., Kellermann, M., Klingebiel, M., Lonardi, M., Lucke, J., Luebke, A. E., Maahn, M., Maherndl, N., Maturilli, M., Mayer, B., Mayer, J., Mertes, S., Michaelis, J., Michalkov, M., Mioche, G., Moser, M., Müller, H., Neggers, R., Ori, D., Paul, D., Paulus, F. M., Pilz, C., Pithan, F., Pöhlker, M., Pörtge, V., Ringel, M., Risse, N., Roberts, G. C., Rosenburg, S., Röttenbacher, J., Rückert, J., Schäfer, M., Schaefer, J., Schemann, V., Schirmacher, I., Schmidt, J., Schmidt, S., Schneider, J., Schnitt, S., Schwarz, A., Siebert, H., Sodemann, H., Sperzel, T., Spreen, G., Stevens, B., Stratmann, F., Svensson, G., Tatzelt, C., Tuch, T., Vihma, T., Voigt, C., Volkmer, L., Walbröl, A., Weber, A., Wehner, B., Wetzel, B., Wirth, M., and Zinner, T.: Overview: quasi-

https://doi.org/10.5194/egusphere-2026-6201
Preprint. Discussion started: 3 November 2026
© Author(s) 2026. CC BY 4.0 License.

Lagrangian observations of Arctic air mass transformations – introduction and initial results of the HALO–($\mathcal{AC}$)^3 aircraft campaign, Atmospheric Chemistry and Physics, 24, 8865–8892, https://doi.org/10.5194/acp-24-8865-2024, 2024.

Yang, C. A., Diao, M., Gettelman, A., Zhang, K., Sun, J., McFarquhar, G., and Wu, W.: Ice and Supercooled Liquid Water Distributions Over the Southern Ocean Based on In Situ Observations and Climate Model Simulations, Journal of Geophysical Research: Atmospheres, 126, e2021JD036045, https://doi.org/10.1029/2021JD036045, 2021.

Yang, J., Qin, Z., Deng, Y., Chen, M., Jing, X., Yin, Y., Lu, C., Chen, B., Zhang, B., and Bao, X.: On the Cluster Scales of Hydrometeors in Mixed-Phase Stratiform Clouds, Geophysical Research Letters, 51, e2024GL108166, https://doi.org/10.1029/2024GL108166, 2024.

Young, K. C.: The Role of Contact Nucleation in Ice Phase Initiation in Clouds, Journal of the Atmospheric Sciences, 31, 768–776, https://doi.org/10.1175/1520-0469(1974)031%3C0768:TROCNI%3E2.0.CO;2, 1974.

Zhang, M., Liu, X., Diao, M., D'Alessandro, J. J., Wang, Y., Wu, C., Zhang, D., Wang, Z., and Xie, S.: Impacts of Representing Heterogeneous Distribution of Cloud Liquid and Ice on Phase Partitioning of Arctic Mixed-Phase Clouds with NCAR CAM5, Journal of Geophysical Research: Atmospheres, 124, 13071–13090, https://doi.org/10.1029/2019JD030502, 2019.